DATES AND RATES OF ENDO-EXORHEIC DRAINAGE DEVELOPMENT: INSIGHTS FROM FLUVIAL TERRACES (DUERO RIVER, IBERIAN PENINSULA)

Laura Rodríguez-Rodríguez[1, 2*], Loreto Antón[3], Ángel Rodés[4], Raimon Pallàs[5], Daniel García-Castellanos[6], Ivone Jiménez-Munt[6], Lucía Struth[6], Laëtitia Leanni[7], ASTER Team[7]

[1] Departamento de Ciencias de la Tierra y Física de la Materia Condensada, Universidad de Cantabria, Avenida de los Castros 48, 93005 Santander, Spain.

[2] Laboratoire de Géographie Physique (UMR 8591, CNRS), 1 Place Aristide Briand 92195 Meudon, France.

[3] Universidad Nacional de Educación a Distancia (UNED), Departamento de Ciencias Analíticas, Senda del Rey 9, Madrid, Spain.

[4] NERC Cosmogenic Isotope Analysis Facility, Scottish Universities Environmental Research Centre, East Kilbride G75 0QF United Kingdom.

[5] Institut de Recerca Geomodels, RISKNAT Group, Departament de Dinàmica de la Terra i de l'Oceà, Universitat de Barcelona, Martí i Franques s/n, Barcelona, Spain.

[6] Institut de Ciències de la Terra Jaume Almera, ICTJA-CSIC, Solé i Sabaris s/n, Barcelona, Spain.

[7] Aix Marseille Université, CNRS, IRD, INRA, Coll France, UM34 CEREGE, Technopôle de l'Environnement Arbois-Méditerranée, BP80,13545 Aix-en-Provence, France. [ASTER Team: Georges Aumaître, Didier Bourlès, Karim Keddadouche]

[*] laura.rodriguezr@unican.es (Corresponding author: L. Rodríguez-Rodríguez)

Abstract

Fluvial terraces are valuable records to study and characterize landscape evolution and river response to base level lowering, and to decipher coupled responses between fluvial incision and regional tectonics. The opening of closed basins has a strong impact on fluvial dynamics, as it involves an abrupt base level lowering that accelerates landscape fluvial dissection. This study focuses on the time response of the Duero Basin, the largest and best preserved among the Cenozoic basins of the Iberian Peninsula, to exorheism. Fluvial incision due to basin opening has developed up to 13 un-paired strath terraces along the south margin of the Duero river, distributed at relative heights up to +136–128 m compared to the modern floodplain. Paired ^{10}Be–^{26}Al cosmogenic isotope depth profiles from six fluvial terraces, located ca. 30 to 80 km upstream from the opening zone, suggest Pleistocene ages for almost the entire fluvial terrace staircase (from T3 at +112–107 m, to T12 at +13–11 m). The terrace density and the total lowering of the terrace surface, key parameters in limiting terrace exposure ages, were estimated based on field and geomorphological data. Apparent burial durations and basin denudation rates deduced from inherited ^{10}Be–^{26}Al concentrations provide valuable information on basin evolution. Apparent basin denudation rates remained relatively low (<3–6 m·Ma^{-1}) during the Pliocene, and doubled (8–13 m·Ma^{-1}) during the Early Pleistocene (ca. 2–1 Ma) possibly showing a lower proportion of recycled sediments. Time averaged incision rates deduced from terraces in the study area and along some tributaries show that incision rates are higher close to the opening site (122 to <250 m·Ma^{-1}) than towards the upstream part of the catchment (88–68 m·Ma^{-1}), evidencing the retrogressive travel of the erosive wave nucleated at the opening site.

1. Introduction

Endorheic basins (also named closed, intermountain, or internally-drained basins) are depressions lacking any water outflow towards the ocean. They constitute valuable records for understanding the evolution and dynamics of surface processes on a range of spatial scales, as they trap sediments until they eventually become externally drained (exorheic), then excavating and exposing their sedimentary record and forming planation surfaces and fluvial terraces, which allows deciphering landscape evolution (García-Castellanos et al., 2003; Yu et al., 2014; He et al., 2017). Investigating how basins evolve after an endo-exorheic transition is key for understanding long-term landscape evolution (at geologic timescale) and for elucidating the mechanisms by which large basins recover a steady state profile. This is most dramatically expressed in the event of large drainage changes caused by fluvial captures, by sediment/water overfilling of basins that leads to basin spillover, or by a combination of these mechanisms (Spencer and Pearthree, 2001; García-Castellanos and Larrasoaña, 2015; Richardson et al., 2008; Heidarzadeh et al., 2017). For example, based on apatite fission track analysis and stratigraphic sections, Richardson et al. (2008) found that the Sichuan Basin (central China) underwent accelerated widespread erosion of 1 to 4 km of overlying sedimentary material after the Yangtze River started excavating the Three Gorges. Similarly, the Ebro Basin (NE Spain) underwent the excavation of up to a kilometer of sediment after its endorheic lake system was captured by or spilled over the Ebro River ca. 8-12 Ma ago (García-Castellanos et al., 2003). Fluvial terrace architecture is key to understand how fast large basins might respond after an endo-exorheic transition and which factors control how the wave of incision is transmitted upstream. The review work of Demoulin et al. (2017) stands out that fluvial terrace patterns and timing of fluvial incision are essential information to isolate the effects of other driving factors for erosion that might be also involved in terrace formation such as tectonics, climate variations, and other non-tectonic factors (such as bedrock lithology). However, few studies focus on continental-scale drainage reorganization and, within those, most studies lack rigorous age control to allow accurate insights into erosion rates and the timing of large-scale landscape modification.

The Iberian Peninsula is known for the occurrence of several large-scale foreland basins formed during the Alpine Orogeny that evolved as closed basins during a significant part of the Cenozoic (Friend and Dabrio, 1996). These basins later became externally drained towards the Atlantic Ocean and the Mediterranean Sea, exposing their infill sequences by fluvial down-cutting in response to basin opening (Figure 1).

Santisteban and Schulte (2007) reviewed fluvial terrace patterns in the major Iberian basins (Duero, Ebro, Tagus, Guadalquivir and Guadiana) and concluded that the time of incision and river response to basin opening is highly variable depending on local/regional climate, glacio-eustatic sea-level changes, and local/regional tectonics. Hence, while some basins such as the Ebro Basin have suffered remarkable erosion of their infill sequence (García-Castellanos and Larrasoaña, 2015), others remain relatively intact. For example, the Duero Basin stands a transient river profile since the endo-exorheic transition (Antón et al., 2012, 2014; Figure 1), recording scarce total denudation due to fluvial entrenchment caused by base level lowering (Antón et al., 2019). A cross comparison between the morphometric indices and knickpoint distribution in the Ebro and Duero basins suggests a short-term aggressive role of the Ebro network (responsible for the westward migration observed in the water divide that separates both basins), but a large-scale aggressor role for the Duero over the Ebro in the long-term based on chi-analysis (Struth et al., 2019). Particularly, the Duero river displays two trains of knickpoints that propagate differently through the soft Cenozoic sediment cover and the Paleozoic crystalline bedrock (Struth et al., 2019), consistently with the few incision rates available in the Arlanzón and Esla tributaries (Moreno et al., 2012; Schaller et al., 2016a). Either a younger opening age for the Duero Basin compared to other Iberian basins (> 3 Ma according to Antón et al., 2019; ~3.7–1.8 Ma according to Cunha et al., 2019; 1.1–1.9 Ma according to Silva et al., 2017) and/or the resistant lithology that configures the Duero basin fringe (Struth et al., 2019) could explain the differences observed in fluvial entrenchment in response to sudden base-level lowering caused by an endo-exorheic transition. Here, we target a sequence of thirteen inset fluvial strath terraces formed in response to the Duero endo-exorheic transition, which are now hanging at heights up to +136–128 m above the modern floodplain (Rodríguez-Rodríguez et al., 2020; Figure 2). The sequence is preserved at the western end of the Cenozoic Duero Basin (CDB), along the 90 km-long reach placed ca. 30 km upstream from the major Arribes knickzone (Figure 1). The Arribes knickzone is excavated in the Paleozoic crystalline bedrock, along the WCB (Western fringe of the Cenozoic Basin) which separates the Duero Lower Reach (DLR) from the Cenozoic sedimentary infill of the CDB (Antón et al. 2012; Figure 1). We fitted the Combined Surface Exposure-Burial Dating (CSEB) model to our ^{10}Be and ^{26}Al depth-profile data in order to produce a numerical geochronology of six terraces belonging to the Duero fluvial staircase, allowing us to discuss: (i) terrace depositional ages; (ii) changes in denudation rates at basin scale over time; (iii) fluvial incision rates in response to base level lowering and fluvial entrenchment, and (iv) discuss the upstream transmission of the erosion wave caused by the endo-exorheic transition.

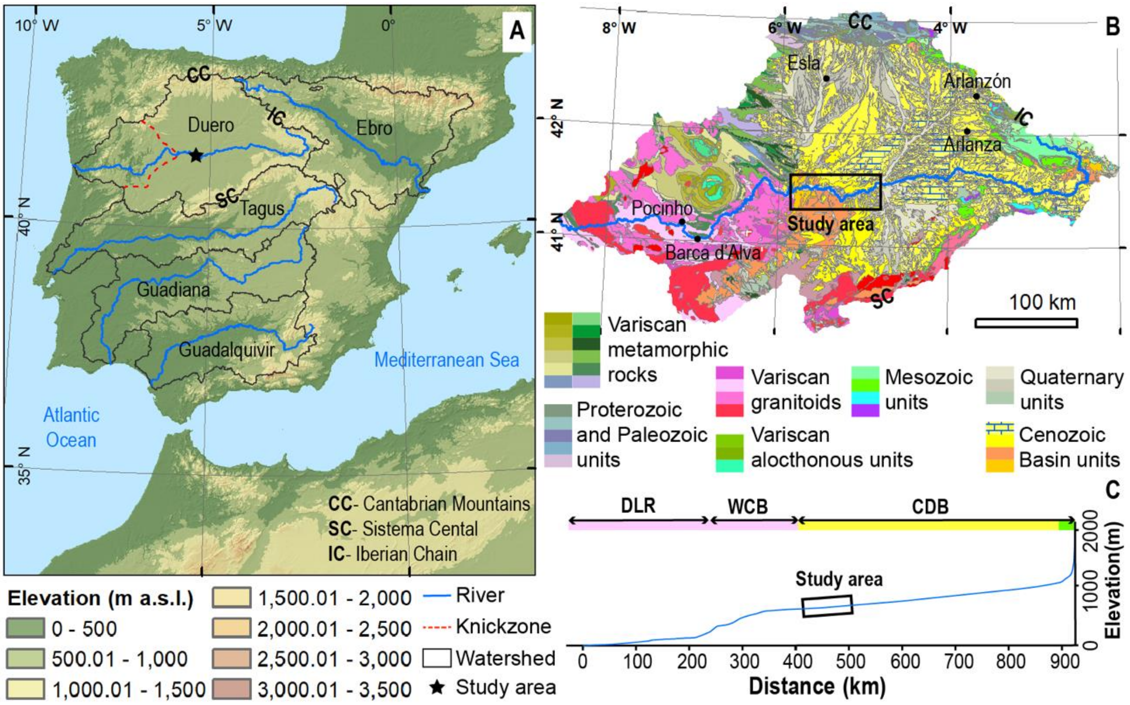

Figure 1.- The Cenozoic Duero Basin (CDB) is the largest Iberian basin that best-preserves both the pre-opening topography and the endorheic sedimentary infill sequence (Antón et al., 2012, 2019). The CDB is limited by the Cantabrian Mountains to the north, the Iberian Chain to the east, the Sistema Central to the south, and the Western fringe of the Cenozoic Basin to the west (WCB). The transient long-profile of the Duero river shows a knickzone along the WCB (excavated in the Paleozoic crystalline bedrock), which separates the Duero Lower Reach (DLR) from the Cenozoic sedimentary infill of the CDB (mostly composed by alluvial detrital conglomerate and sandstone capped by lacustrine carbonate and evaporitic units). Geologic map source: http://mapas.igme.es/gis/rest/services/Cartografia_Geologica/IGME_EP_Geologico_1M_2018/MapServer (last accessed on April 2020).

2. Geologic and geomorphologic background of the study area

The Duero Basin is the largest among the Iberian Cenozoic basins: ~50000 km^2 in sediment-covered area and 90400 km^2 in total catchment area (Antón et al., 2019). It acted as foreland basin for the Cantabrian Mountains during the Eocene (Alonso et al., 1996) and for the Sistema Central between the Oligocene and Miocene (Capote et al., 2002), accumulating as much as 3 km of sediments (Gómez-Ortiz et al., 2005). The youngest geologic formation sedimented in endorheic conditions, named the Páramo Formation, is mostly composed by extensive carbonate facies (mostly limestone, marl and gypsum) that suggests major expansion of lake environments at the basin's depocenter during the middle and upper Miocene (Alonso-Zarza et al., 2002). Based on magnetostratigraphic analysis, the top of the Páramo Formation was assigned a Tortonian age (9.7–9.6 Ma according to Krijgsman et al., 1996; ~9.1 Ma according to Beamoud et al., 2006). In contrast, mammal assemblages found at the youngest carbonate unit of this formation (the Upper Páramo Limestone, or UPL) yielded Vallesian ages in the southwest part of the basin (where the record is less complete), while Turolian ages have been reported for fluvial deposits near the base of the sequence at the basin center, which might point to a Pliocene age for the top of the UPL (Alonso-Gavilan et al., 1989; Mediavilla and Dabrio, 1989; Alonso-Zarza et al., 2002 and references therein). However, Santisteban et al. (1997) have interpreted these fluvial deposits as related to the first stages of fluvial dissection already in exorheic conditions. A detailed analysis of erosion surfaces in the eastern sector of the basin (Sierra de Atapuerca in the Iberian Chain) reveals up to four erosional surfaces, the youngest formed after the Duero Basin opened to the Atlantic (Benito-Calvo and Pérez-González, 2007). It laterally connects with the Lower Páramo Surface (LPS in Figure 2), developed on top of the Lower Páramo Limestone unit (or LPL) due to differential exposure in response to fluvial dissection after the basin opening during the Pliocene-Pleistocene (Benito-Calvo and Pérez-González, 2007). An opening age of ~1.1 to 1.9 Ma has been proposed based on a cross-comparison between the fluvial terrace staircases preserved in the Duero and the Tagus basins, henceforth attributing the full sequence of fluvial terraces to the Pleistocene (Silva et al., 2017). However, the age-height transfer curve reported for the Duero river in their work was supported on the few numerical ages available for the Arlanzón tributary, close to the source area of sediments in the Iberian Chain (Figure 1). Finally, an older opening age range of ~3.7–1.8 Ma has been recently reported based on an extrapolation of incision rates derived from strath terraces hanging at +53–48 m (360–>230 ka), +34–27 m (57 ka) and +17–13 m (39–12 ka) between Pocinho and Barca d'Alva (Cunha et al., 2019), downstream of the Arribes knickzone, in the upper end of the Duero Lower Reach (DLR; Figure 1).

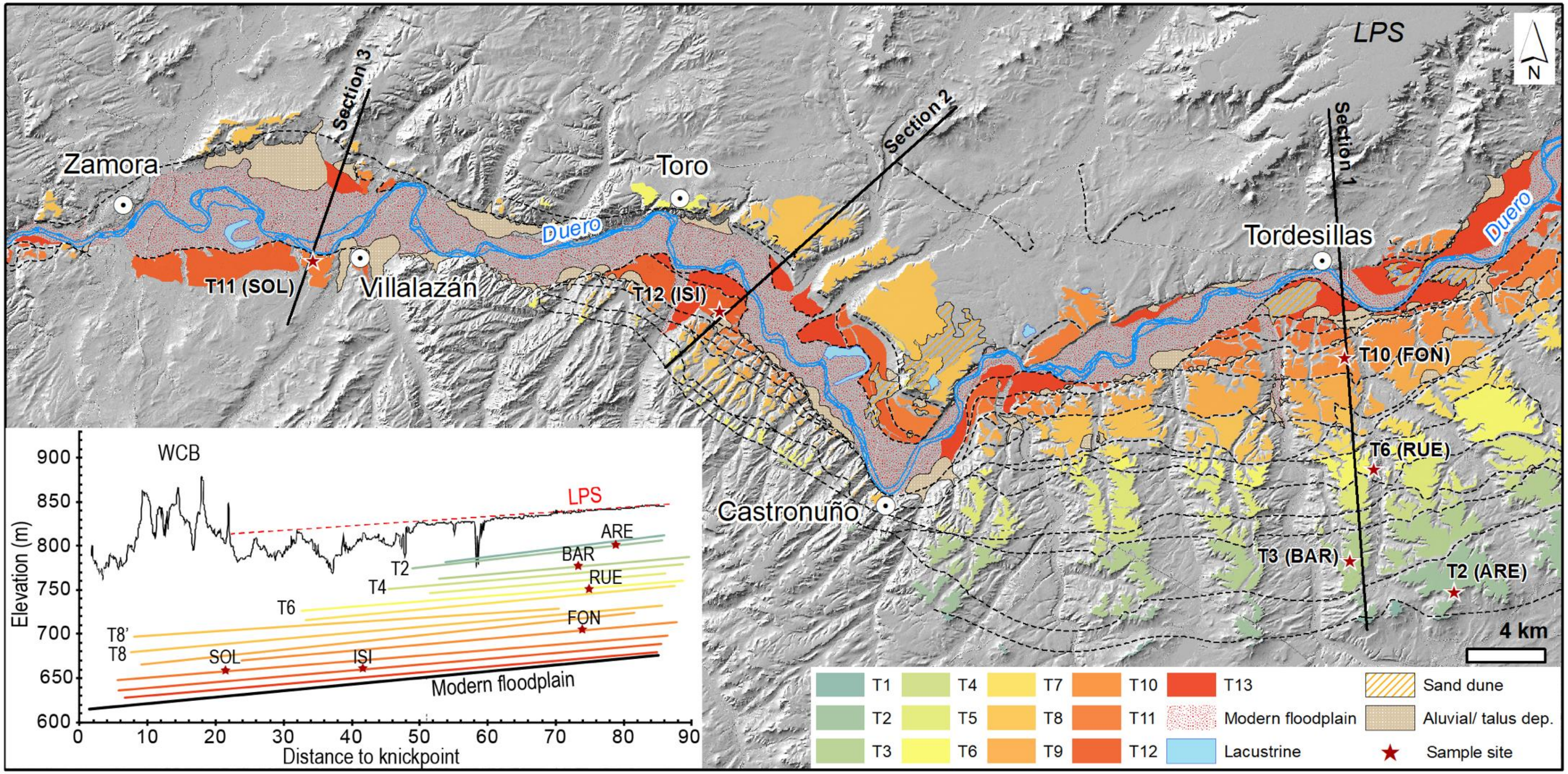

Figure 2.- Geomorphological map of the fluvial terrace staircase developed by the Duero River upstream the Arribes knickpoint. Terrace sample site locations are shown both in the map and along the reconstructed former river profiles based on statistical analysis of terrace surface points extracted from a high-resolution digital elevation model (Rodríguez-Rodríguez et al., 2020). The swath profile of maximum elevation shows the topographic signature of the LPS erosional surface, presumably linked to the initial emptying of the basin after the endo-exorheic transition.

Although the precise location of the opening point for the CDB drainage is unknown, there is a general consensus about its location at the WCB (Silva et al., 2017 and references therein; Figure 1). This work refers to an opening area located at the Arribes knickzone (ca. 20-50 km downstream from Zamora; Figure 2) where resistant bedrock, composed by igneous and metamorphic rocks, controls the initiation and progression of the continental scale drainage reorganization at the uppermost CDB (e.g. Struth et al., 2019). The study area covers the lowermost 90 km-long reach of the upper Duero river placed immediately upstream the Arribes knickzone, in the Spanish regions of Valladolid and Zamora. Modern climate is characterized by mean annual precipitation of 366–478 mm (https://sig.mapama.gob.es/siga/, accessed on August 2019), with a marked dry season in summer. Mean annual temperature is ~12 ºC, annually displaying less than 49 days of winter temperatures equal or below 0ºC (mean temperature minima values in January are 2.5–5ºC) and reaching maxima temperature values in the range 22.5–25ºC during the summer season (http://www.aemet.es/es/serviciosclimaticos/datosclimatologicos/atlas_climatico/visor_atlas_climatico#enlaces_asociados, last accessed on April 2020). Fluvial terraces crop out as un-paired strath terraces formed by incision of the Duero River in the endorheic infill sequence in response to the base level lowering linked to the endo-exorheic transition, forming successive bedrock stairs capped with fluvial sediments up to 2–7 m thick. The elevation difference between the LPS (preserved in the north margin of the river) and the modern floodplain suggests that total incision overcomes 180 m (Figure 2). Fluvial terraces are preferentially preserved along the south margin of the river, extending as far as 18 km south from the modern channel and hanging above the modern floodplain at relative heights of: +136–128 m (T1); +130–124 m (T2); +110–109 m (T3); +104–101 m (T4); +95–91 m (T5); +88–81 m (T6); c. +77 m (T7); +79–59 m (T8'); +60–55 m (T8); +51–44 m (T9); +40–35 m (T10); +30–10 m (T11); +18–12 m (T12); and +9–3 m (T13; Rodríguez-Rodríguez et al., 2020). The staircase sequence is fully represented in the eastern half of the study area, east of Castronuño village, while only the intermediate and lowest terrace levels are present between Castronuño and the Arribes knickzone. This pattern is possibly related to the occurrence of higher incision rates close to the opening site than those recorded upstream over the time period when terraces T1 to T9 were being deposited. This would explain the more extensive terrace remnants and the higher number of terrace levels upstream Castronuño than between Castronuño and the Arribes knickzone. Fluvial long-profiles reconstructed through statistical analysis of terrace surface points extracted from high resolution LiDAR digital elevation models revealed upstream diverging patterns in the highest terraces, and downstream diverging to parallel patterns in the intermediate and lowest terrace levels (Figure 2; Rodríguez-Rodríguez et al., 2020).

3. Methodology

The cosmogenic nuclide dating technique applied to sediment landforms relies on the measurement of various cosmogenic nuclides produced and stored inside the lattice of a target mineral by the interactions with the cosmic rays (Gosse and Phillips, 2001). The pair of cosmogenic nuclides most frequently used to study alluvial landforms is ^{10}Be–^{26}Al, as they are produced in the same target mineral (quartz) at a ratio of ~6.75 largely independent from altitude and latitude (Dunai, 2010). Once sediments are buried deep enough to be fully shielded from cosmic radiation, their initial concentrations start to decay at a pace of 4.9975 x10^{-7} a^{-1} for ^{10}Be (Chmeleff et al., 2010) and 9.83 x10^{-7} a^{-1} for ^{26}Al (Nishiizumi, 2004). If sediments have been sufficiently exposed before being buried, the residual concentration of paired ^{10}Be–^{26}Al cosmogenic nuclides measured in deep samples can be used to solve for the burial time (Granger and Muzikar, 2001).

In this study, the timing of river incision and fluvial terrace formation was constrained through the CSEB model proposed by Rodés et al. (2014), which considers the possible occurrence of complex exposure-burial histories before the final deposition of sediments takes place. It is expressed as function of: (i) the apparent pre-depositional average exhumation rate at the catchment source area; (ii) the apparent pre-depositional burial time; (iii) the local denudation rate; and (iv) the terrace surface age.

Exhumation rates are considered apparent because, although most reworking processes change the ^{10}Be-^{26}Al signature towards concentrations that suggest lower erosion rates, there could be scenarios where sediments have been recycled after a long period of burial and, hence, the ^{10}Be-^{26}Al signature would solely reflect the last erosion rate. In any case, the ^{10}Be-^{26}Al signatures shall reflect an apparent erosion rate and an apparent burial duration, both corresponding to an unbalanced average of all erosion stages occurred and their respective durations.

3.1. Terrace depth profile sampling

In order to constrain as much as possible the age of the Duero river terrace staircase, the thickest terrace sequences, displaying well-preserved top surfaces, were preferentially targeted for deep profile sampling. We tried to cover the greatest number of terrace levels distributed over the central CDB, across sections 1, 2, and 3 (located ca. 30-80 km eastward from the WCB; Figure 2). Potential terrace sections were located using high-resolution LiDAR digital elevation models and aerial imagery (https://www.cnig.es; last access on June 2016), and visited in the field to verify that sediment thickness was greater than 4 m. Paired ^{10}Be–^{26}Al cosmogenic nuclides depth profiles were sampled from sections of six fluvial terraces of the Duero river staircase, including a total number of 31 sediment samples taken mostly from sections at open cast quarries dedicated to gravel extraction (named Arentis, Barbado Martín, Foncantín, Jose Isidro Torres, and Sola e Hijos). The following terrace levels were sampled (Figures 2 and 3): T2 (code ARE; 2 samples), T3 (code BAR; 3 samples), T6 (code RUE; 6 samples), T10 (code FON; 6 samples), T11 (code SOL; 7 samples), and T12 (code ISI; 6 samples). We collected 6–7 sediment samples per terrace profile exponentially spaced from 20–30 cm below the surface down to 4.25–5 m (Figure 4 and Table I). In the oldest terraces (T2 and T3), the probability of finding saturated profiles was considered to be high and, hence, only the deepest samples of the profile (at 3 and 4.50–5.50 m depth, respectively) were taken. The geographic location and altitude of each sampling site was determined in the field by GPS positioning. The maximum surface lowering of sampled terrace remnants was inferred using topographic sections passing through each sampling site, assuming that terrace top surfaces were originally flat. For this purpose, a 3 m cell-size resolution digital elevation model derived from the LiDAR datasets from the Spanish National Institute of Geography was used. Fluvial sediment facies were described at each sampling location. A description of the main soil characteristics (number of horizons, thickness, presence of pedogenic calcrete) is also provided to address age interpretations (in terms of possible hiatuses during terrace aggradation), and to offer an alternative surface lowering scenario for the sampled terraces. Regarding the grain size fraction sampled, given that fluvial deposits in this area are cobble- and pebble-dominated, the pebble fraction in the range 2 mm–2 cm in diameter was targeted in all cases, ensuring that more than 200 particles per sample were collected.

Density values assigned to fluvial sediments might have a strong impact in the final age model (Rodés et al., 2011). Thus, twenty-three density measurements were performed in the field for the various fluvial terrace materials identified and sampled, obtaining results in the range 1.49–2.31 $g \cdot cm^{-3}$, and an average density value of 1.72 ± 0.2 $g \cdot cm^{-3}$ (further details are provided in the supplementary material). Based on these results, a range of density values of 1.52–1.92 $g \cdot cm^{-3}$ has been introduced in the models, which is in good agreement with reference density values provided for dense coarse granular soils in some engineering manuals (e.g. González de Vallejo, 2002).

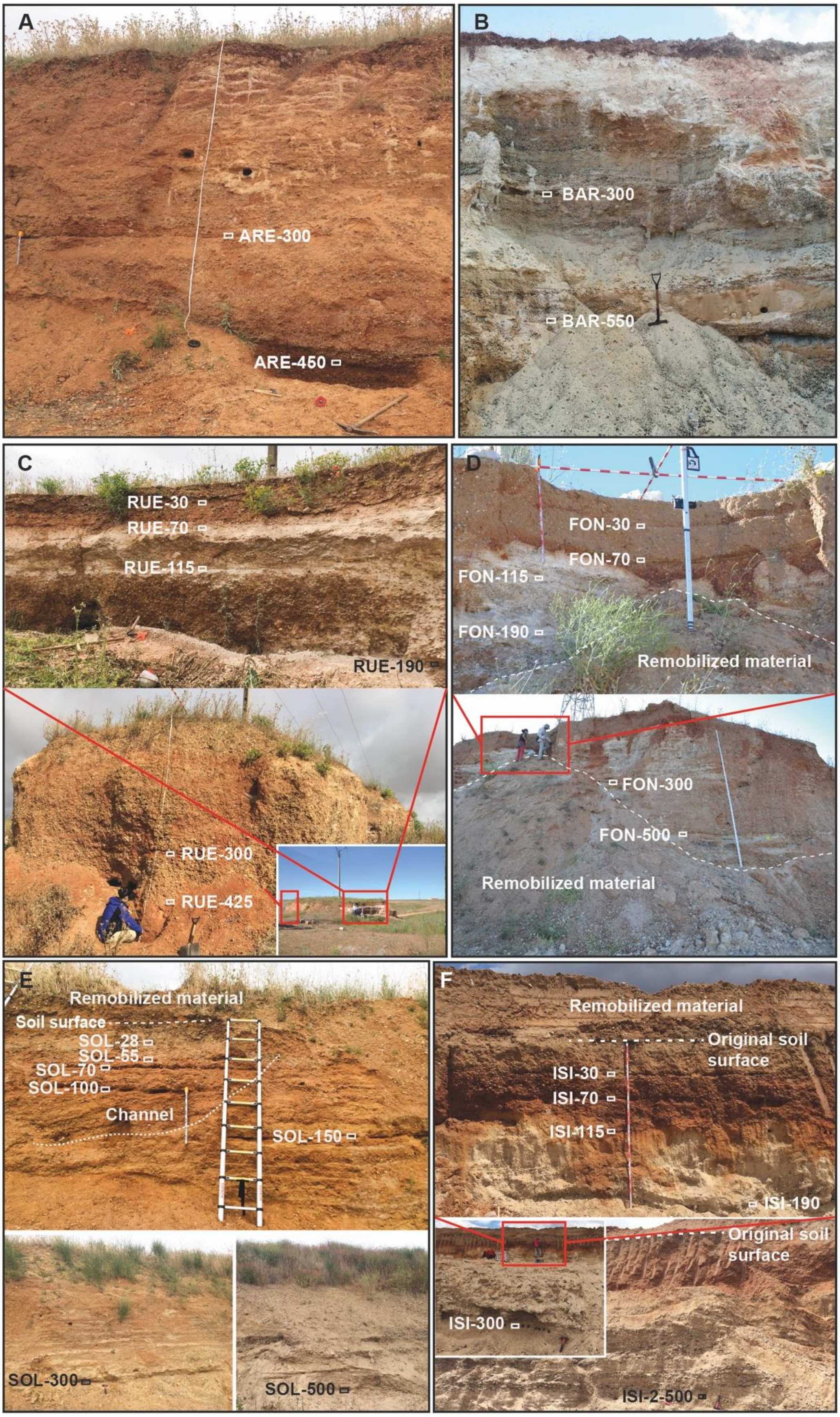

Figure 3.- Terrace sampling sections: A) T2 at Arentis quarry; B) T3 at Barbado Martín quarry; C) T6 at an old extraction area close to Rueda; D) T10 at Foncastin quarry; E) T11 at Sola e Hijos quarry; and F) T12 at Isidro quarry. Labels indicate sampling depths expressed in centimeters.

3.2. Sample treatment and AMS measurement of Be and Al ratios

Fluvial sediment samples were crushed and sieved at the *Departament de Dinàmica de la Terra i de l'Oceà* (*Universitat de Barcelona*) in order to reduce the grain size to 1mm–250 µm in diameter, optimal for doing the chemical processing. Sample treatment was conducted at *Laboratoire National des Nucléides Cosmogéniques* (LN2C) – *Centre Européen de Recherche et d'Enseignement des Géosciencies de l'environnement* (CEREGE, Aix-en-Provence). The extraction of magnetic dark mineral grains was done using a Frantz magnetic separator and applying a magnetic field intensity of 1A. Sample cleaning involved carbonate removal with hydrochloric acid and several acid leaching baths with a mixture of hydrochloric and hexafluorosilicic acids. The isolation and purification of quartz was done through four etching bathes with hydrofluoric acid to ensure a full removal of atmospheric ^{10}Be. Once cleaned, quartz samples (20–30 g) were spiked with ~100 mg of a phenakite carrier solution with a concentration of 3025 ± 9 $\mu g \cdot g^{-1}$ of ^{9}Be before total dissolution in hydrofluoric acid. Samples were aliquoted for the ICP-OES analysis of the natural ^{27}Al concentration in the samples. Given the low natural concentration of ^{27}Al in the samples (mean value of 2.03 ± 0.66 ppm), a volume of 750–2100 mg of a commercial VWR Prolabo spike solution with a ^{27}Al concentration of 981 ± 4.91 $\mu g \cdot g^{-1}$ was added to each sample to ensure a final Al sample of ~2 mg. Beryllium and aluminum were separated from the solution by successive column chromatography using anionic (DOWEX 1X8) and cationic (DOWEX 50WX8) resins. The recovered Be and Al solutions were taken to pH ~8.5 to precipitate the hydroxides, that were subsequently washed in slightly basic solutions. After drying the last precipitates in porcelain crucibles, samples were heated in the oven at 800ºC during one hour. Resultant BeO and Al_2O_3 precipitates were mixed with niobium and silver powder to perform the AMS measurements at the French AMS National Facility ASTERisques, located at CEREGE (Aix-en-Provence). Beryllium measurements were calibrated against the reference material NIST–SRM4325 [nominal value of (2.79 ± 0.03) x10^{-11} equivalent to 07KNSTD within rounding error], while aluminum measurements were calibrated against the in-house standard SM-Al-11 [nominal value of (7.401 ± 0.064) x10^{-12}] (Arnold et al., 2010). The ASTER ^{26}Al standard (the only available ^{26}Al standard cross-calibrated against the primary standards certified by a round-robin exercise) yields a ratio of (7.554 ± 0.104) x10^{-12} when measured against the ^{26}Al KNSTD10650 standard, 2.1% higher than the nominal value (Rixhon et al., 2011). The SM-Al-11/07KNSTD standardization used in this work implies a ^{26}Al/^{10}Be production ratio of 6.61 ± 0.52 (Braucher et al., 2011), which is in good agreement with the ~6.75 ratio broadly accepted in the literature (Dunai, 2010). Reported analytical uncertainty (1 σ) includes: (i) an external uncertainty of ~0.5% that accounts for all effects contributing to ASTER's variability (Arnold et al., 2010); (ii) a counting statistics uncertainty of ~3% (~1,500 events) related to the cumulative number of ^{10}Be events and ~4% (~850 events) related to the number of ^{26}Al events acquired during AMS measurements; and (iii) the uncertainty linked to the chemical blank correction. The reported analytical uncertainty of the aluminum concentrations also accounts for the errors associated with the ICP-OES analysis (model Thermo iCAP 5000 Series) carried out at CEREGE. Long-term AMS measurements of procedural blanks yield a background ratio of (2.4 ± 1.5) x10^{-15} for ^{10}Be/^{9}Be and (2.2 ± 2.0) x10^{-15} for ^{26}Al/^{27}Al (Bourlès, personal communication). However, the procedural blank in our dataset yielded ratios of 3.13 x10^{-14} for ^{10}Be/^{9}Be and 8.76 x10^{-16} for ^{26}Al/^{27}Al. We verified that the unusually high ^{10}Be/^{9}Be ratio observed in the blank responds to a ^{10}Be contamination of the ^{27}Al carrier solution (~3.507 x10^{-12} ppm of ^{10}Be) that has been corrected in all samples.

Table I.- Location coordinates (in decimal degrees) and terrace top surface elevation at the sampled terrace depth profiles and measured ^{10}Be and ^{26}Al concentrations.

Terrace level	**Sample**	**Depth (cm)**	**[Be-10] (10^3 at·g^{-1})**	**[Al-26] (10^3 at·g^{-1})**
T2 41.3522, -4.9159 800 m a.s.l.	ARE-300	300 ± 3	214.7 ± 7	462 ± 31
	ARE-450	450 ± 2	188.5 ± 6.1	263 ± 21
T3 41.3660, -4.9792 779 m a.s.l.	BAR-300	300 ± 4	340 ± 12	974 ± 55
	BAR-550	550 ± 3	246.5 ± 8.2	302 ± 22
	BAR-02-550	550 ± 2	225 ± 7.5	312 ± 27
T6 41.4064, -4.9643 753 m a.s.l.	RUE-030	30 ± 2	3487 ± 69	15500 ± 370
	RUE-070	70 ± 2	1867 ± 52	5260 ± 170
	RUE-115	115 ± 2	1325 ± 31	4440 ± 140
	RUE-190	190 ± 3	691 ± 24	2102 ± 75
	RUE-300	300 ± 3	436 ± 14	693 ± 37
	RUE-425	425 ± 2	461 ± 14	990 ± 43
T10 41.4584, -4.9865 707 m a.s.l.	FON-030	30 ± 2	1824 ± 48	8420 ± 260
	FON-070	70 ± 2	1168 ± 33	5500 ± 170
	FON-115	115 ± 2	874 ± 25	4210 ± 140
	FON-190	190 ± 2	557 ± 17	2122 ± 78
	FON-300	300 ± 2	523 ± 16	1717 ± 59
	FON-500	500 ± 2	338 ± 11	1187 ± 65
T11	SOL-028	28 ± 2	1044 ± 29	5580 ± 170

41.4908, -5.6197 656 m a.s.l.	SOL-055	55 ± 2	671 ± 21	3540 ± 120
	SOL-070	70 ± 2	580 ± 19	3340 ± 110
	SOL-100	100 ± 2	612 ± 22	3210 ± 110
	SOL-150	150 ± 2	458 ± 15	2090 ± 68
	SOL-300	300 ± 2	451 ± 15	2081 ± 76
	SOL-500	500 ± 2	368 ± 12	1357 ± 46
T12 41.4735, -5.3685 657 m a.s.l.	ISI-020	20 ± 1	939 ± 29	4070 ± 130
	ISI-040	40 ± 1	787 ± 26	3920 ± 120
	ISI-070	70 ± 2	642 ± 21	2855 ± 100
	ISI-110	110 ± 4	446 ± 14	1955 ± 69
	ISI-190	190 ± 4	376 ± 12	1314 ± 62
	ISI-300	300 ± 5	242.3 ± 8	736 ± 59
	ISI-02-500	500 ± 5	261.6 ± 9	829 ± 45

3.3.CSEB age model

The ^{10}Be and ^{26}Al concentrations measured in the profiles allowed us to model the shape of the theoretical in-situ produced cosmogenic nuclide signature with sample depth since terraces were deposited, and the construction of a chronological framework compatible with the cosmogenic nuclide signature measured. A Monte Carlo simulation of random models distributed in a window of 0–10 Ma was run in MATLAB® to find the chi-square values of the models that best fit the concentrations measured in our profiles. Monte Carlo simulations were run until 300 models fitting the 1-sigma confidence interval were found. Chi-squared minimization was performed for the models fitting the 1-sigma confidence interval (Rodés et al., 2014). The *in situ* production rate of cosmogenic ^{10}Be and ^{26}Al at each sampling site was determined considering the constant production rate model of Stone (2000) and apparent attenuation length values calculated from muonic production rate cross-sections generated using the code from the online calculator formerly known as the CRONUS-Earth online calculator v 2.3 (Balco et al., 2008; Table II). Uncertainties related to cosmogenic nuclides half-life and production rate were not included in age calculations, involving that uncertainties reported for burial durations shall be considered as internal uncertainties. The transmission of half-life and production rate uncertainties would impact the exposure ages by 10% or less, which is negligible compared to uncertainties of the obtained exposure ages.

A first modeling was performed without imposing geological constraints relative to the preservation degree of the surface. However, as the terrace preservation is a key factor in determining individual terraces ages (onset of terrace surface exposure), further models were run limiting the maximum lowering of each surface to better constraint the exposure age of terrace surfaces. Maximum lowering values assumed in the final CSEB age model are discussed in the results section with regards of soil evidence and lowering measurements.

Table II.- ^{10}Be - ^{26}Al local production rates (P) and attenuation lengths (Λ) for spallation (sp), slow muons (sm) and fast muons (fm) according to Stone (2000) and using the code from CRONUS Calc v 2.3 (https://hess.ess.washington.edu; Balco et al., 2008). Catchment production rates were estimated using the average elevation of the source (1300 m) and the same latitude as the sampling sites because the Duero Basin is E-W trending.

Location	**Isotope**	**Psp** (at·g^{-1}·a^{-1})	**Psm** (at·g^{-1}·a^{-1})	**Pfm** (at·g^{-1}·a^{-1})	**Λsp** (g·cm^{-2})	**Λsm** (g·cm^{-2})	**Λfm** (g·cm^{-2})
Basin source	^{10}Be	11.1655	0.0663	0.0491	160	859.1591	1606.500
	^{26}Al	75.3295	0.7522	0.3381	160	859.1591	1606.500
ARE	^{10}Be	7.5358	0.0538	0.0441	160	1002.8100	1775.0137
	^{26}Al	50.8407	0.6105	0.3042	160	1002.8100	1775.0137
BAR	^{10}Be	7.4098	0.0534	0.0439	160	1021.5003	1819.2790
	^{26}Al	49.9910	0.6050	0.3029	160	1021.5003	1819.2790
RUE	^{10}Be	7.2586	0.5028	0.0437	160	1016.4472	1784.2750
	^{26}Al	48.9709	0.5983	0.0433	160	1016.4472	1784.2750
FON	^{10}Be	6.9952	0.0517	0.0433	160	1041.6347	1830.8945
	^{26}Al	47.1941	0.5866	0.2982	160	1041.6347	1830.8945
SOL	^{10}Be	6.7157	0.0506	0.0428	160	1060.3815	1852.4256
	^{26}Al	45.3082	0.5740	0.2950	160	1060.3815	1852.4256
ISI	^{10}Be	6.7175	0.0506	0.0428	160	1060.1647	1852.1961
	^{26}Al	45.3200	0.5742	0.2950	160	1060.1647	1852.1961

4. Results

4.1. Sampled terrace depth profiles: sedimentology and soil characteristics

Terraces T2, T3, T6, and T10 were sampled along cross section 1, located ca. 70-80 km east from the WCB (Figures 4 and 5). Fluvial sediment thickness ranges between 4.2 and 4.7 m in terraces T2 and T6, and reaches up to 7 m in terrace levels T3 and T10 (Figure 4). Fluvial terraces T2 and T3 are lying directly on top of the Miocene bedrock, which locally consists of grey clay and marls. Fluvial sequences sampled in terraces T2, T6 and T10 are composed by reddish grain-supported cobble and gravel sediments with sandy matrix, displaying massive strata or parallel to low-angle bedding, and locally cobble imbrications. Some few centimeters-thick intercalations of sand with sparse gravels are also present, showing parallel bedding (T2 and T6) or planar cross-bedding (T10). These terraces probably represent the stacking of ancient river bars in a braided fluvial system of high flow regime. Meanwhile, the sequence of terrace T3 is richer in sandy intervals compared to T2, T6 and T10. Particularly, T3 is composed by decametric to centimetric sets of sand and gravel sediments showing normal graded stratification, and displaying through cross-bedding close to the base and planar cross bedding towards the top. Thus, sediment architecture in T3 reflects a fluvial system of lower flow energy regime than in terraces T2, T6 and T10.

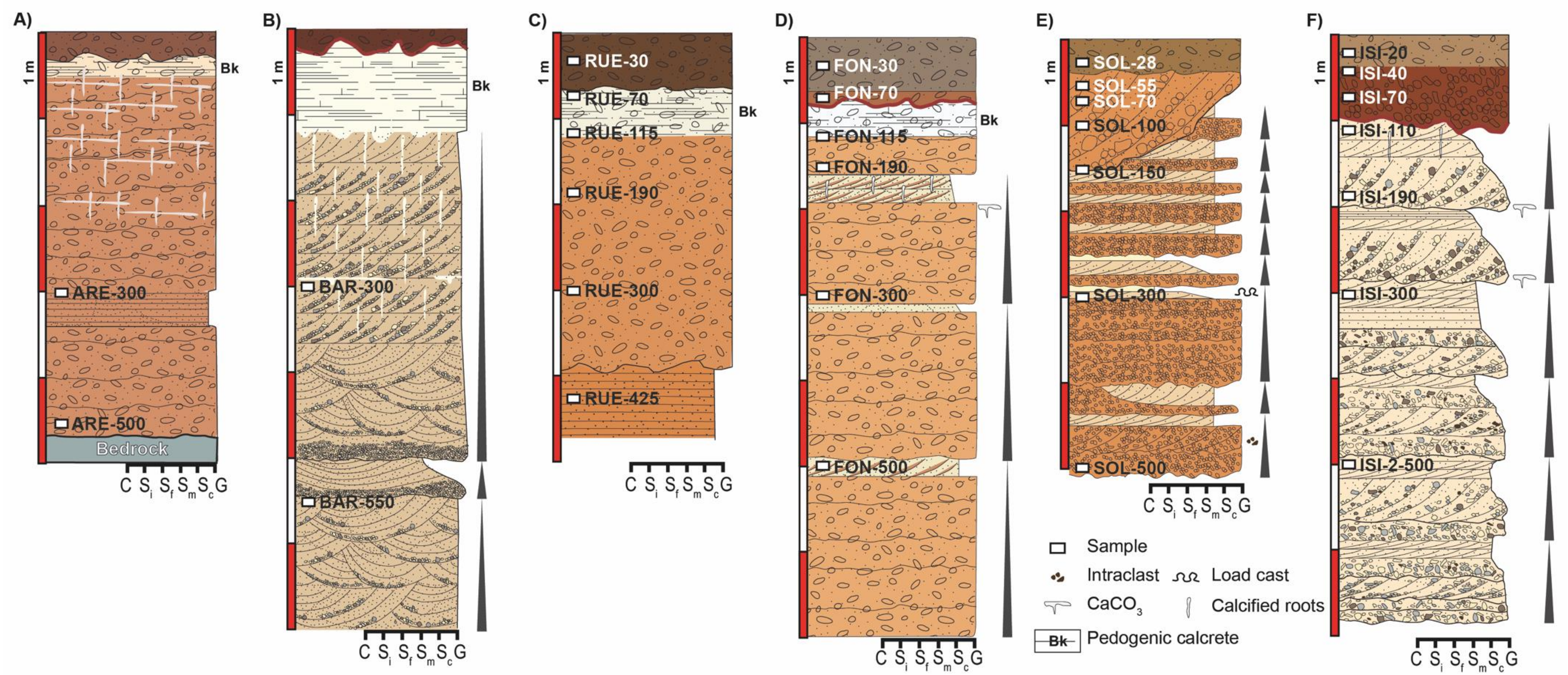

Figure 4.- Stratigraphic sections of the sampled terraces showing the distribution of samples in each terrace profile (grains size key is: C- clay; S_i- silt; S_f- fine sand; S_m- medium sand; S_c- coarse sand; G- gravel): A) T2 at Arentis quarry; B) T3 at Barbado Martín quarry; C) T6 at an old extraction area close to Rueda; D) T10 at Foncastin quarry; E) T11 at Sola e Hijos quarry; and F) T12 at Isidro quarry.

The youngest terraces (in terms of relative age) targeted for sediment depth profile sampling are T11 and T12, respectively sampled at cross sections 2 and 3 placed ca. 22 and 42 km upstream from the Arribes knickzone (Figures 2 and 5). The sequence of T11 at SOL sampling site is 5.5 m-thick and includes alternations of reddish gravel units and yellowish sand and clay intervals arranged as normal graded sequences (Figure 4). The thickness of gravel units decreases from metric-decametric to centimetric beds upwards, mostly showing massive or parallel stratification and eventually displaying cross-bedding and muddy intraclasts. Gravel units alternate with thinner units of coarse-medium sand that gradually decrease in grain size towards the top to fine sand, silt and clay. Deformation structures such as load casts are visible in the clay intervals. Altogether, they are arranged as stacked normal graded sequences. A channel infill cross-cut the sequence previously described in the uppermost 1.5 m of the profile, composed by cross-bedded cobble and gravel sediments with sandy matrix. We interpret the lowest part of the sequence as the floodplain facies adjacent to the river channel infill. Finally, the youngest terrace level sampled, T12, is ca. 7 m in thickness. It is mostly composed by cross-bedded cobble, gravel and coarse sand sediments arranged as normal graded sequences. The uppermost part of the sequence culminates with coarse to medium sand beds displaying parallel or planar cross-bedding. The fluvial flow regime would be comparable or slightly more energetic than during the formation of T3 considering the grain size and sediment structures identified in the field.

Soils in the sampled terraces are generally around 1–1.15 m-thick (T3, T6, T10, T12) independently from their relative age, and exceptionally thinner than 1m in some terraces (0.5 m-thick in T2 and 0.4 m thick in T11; Figure 4) most likely due to post-soil formation erosion. Two similarities were noticed between the soils developed in the sampled terraces. First, the presence of an argillic horizon with intense dark red coloring, which is directly exposed to the surface in the oldest terraces T2 and T3, or at the base of a dark-brown argillic horizon (horizon B) in the intermediate (T6) and low terraces (T10 and T12). Second, the occurrence of a well-developed petrocalcic horizon (cemented by calcium carbonate) below the dark red argillic horizon in terraces T2 (20 cm-thick), T3 (100 cm-thick), T6 (50 cm-thick), and T10 (40 cm-thick), starting at depths of 30-20 cm in the highest terraces (T2-T3) and at 70 cm in T6 and T10 (Figure 4 A-D). It is worth mentioning that these two features are missing in the soil profile at the sampling site of T11, where the soil shows a brown argillic horizon B ca. 40 cm-thick. Previous studies have classified the soils in the study area as Alfisols (Pérez-González, 1982). More specifically they could correspond to Xeralfs, which are typical of Mediterranean-type climate regimes and usually remain dry for extended periods in summer (Soil Survey Staff, 2015).

4.2.Terrace surface preservation and maximum lowering estimates

Across Duero valley profiles passing through the sampling sites show the vertical height of terrace scarps between successive levels (Figure 5). Although their top surfaces are relatively well preserved in the study area, they show evidence of runoff erosion and deflation (like blowout depressions up to 2 m deep and ventifacts), indicating that erosion was locally important. Moreover, terraces might be prone to burial by slope deposits and tributary fans from adjacent terrace levels (Mather et al., 2017), but this is not an issue at our particular sampling sites. In order to constrain the exposure age of terrace surfaces in the CSEB model, we limit the maximum lowering experienced by each surface based on geological evidence.

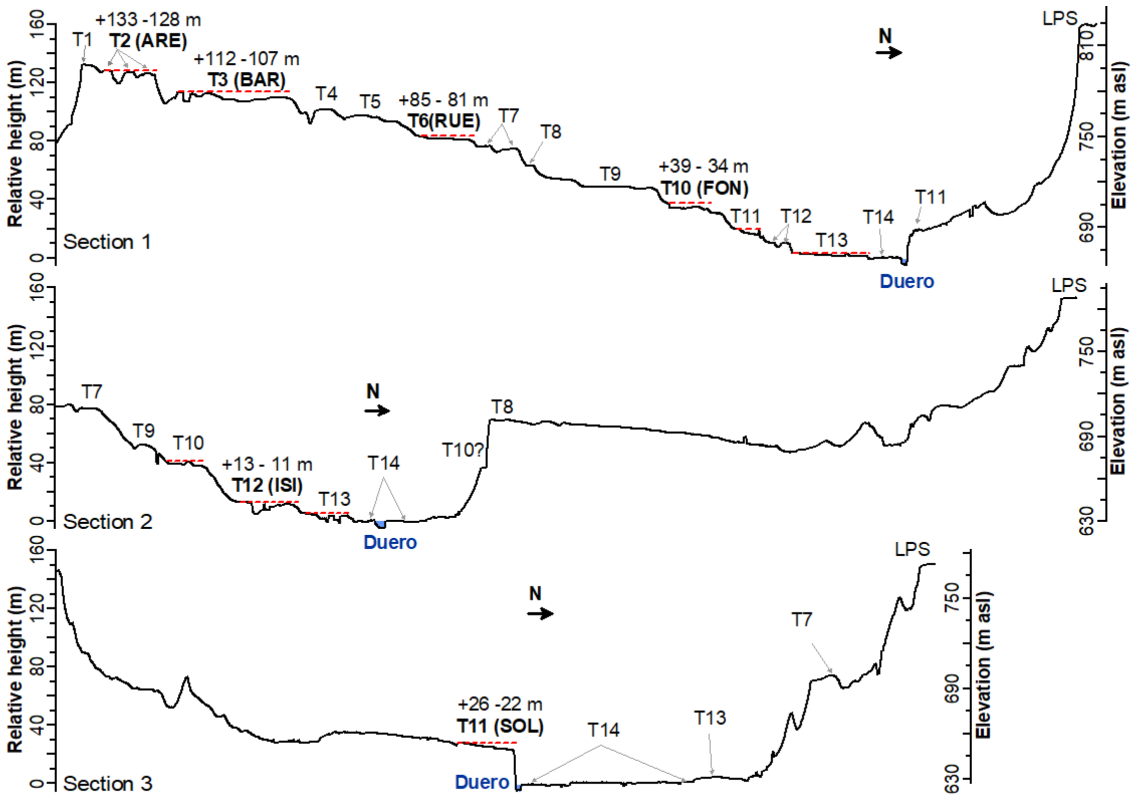

Figure 5.- Sections of the Duero river crossing the sampling sites (see Figure 2 for the exact location of each section). They show the full sequence of terrace levels preserved in each area and the spatial relationships between them and with the modern floodplain (reference level to calculate the relative height) and the LPS erosional surface to the North. Red dashed lines indicate the possible position of original terrace top surfaces, providing a minimum estimate for the post-depositional maximum lowering of the surface.

A first estimate of the true maximum lowering values of the sampled surfaces was done measuring the altitude difference between the terrace top surface at the sampling point and the maximum altitude observed in the surrounding areas of the same terrace outcrop. Assuming that the original terrace surface was flat (represented by red dashed lines in Figure 5), total lowering estimates up to ~5 m for T2 (ARE), ~3.5 m for T3 (BAR), ~3 m for T6 (RUE) and T10 (FON), ~4 m for T11 (SOL), and ~1.5 m for T12 (ISI) were inferred. Additional lowering linked to the erosion of the highest portion of a terrace top surface is difficult to infer due to the lack of indicators. However, since evidence of fill terraces was not found at the studied sites, denudation would be limited to the height difference between the highest sectors of a terrace top surface and the base of an immediately higher terrace. Therefore, no more than ~3 m of additional erosion would be possible in terrace T2 (ARE), ~15 m for terrace T3 (BAR), ~7 m for terrace T6 (RUE), ~8-6 for terrace T10 (FON), and ~5 m for terrace T12 (ISI). In the case of terrace T11 (SOL), the lack of higher terrace levels at Villalazán section makes impossible a direct measurement, but long profile analysis based on terrace levels preserved in the area shows an increasing trend in height difference between terrace levels T10 and T11 towards the WCB, placing the corresponding terrace scarp between ~15–10 m (Rodríguez-Rodríguez et al., 2020). Considering that the maximum thickness of fluvial sediments observed for terrace T10 is 7 m, a total lowering in the range ~8–3 m can be inferred for T11 (SOL).

An alternative scenario of surface lowering was inferred from the soil characteristics observed in the different terraces (number and thickness of horizons preserved, presence of pedogenic carbonates). Terraces T2 to T10 contain pedogenic calcrete horizons (Bk), reaching ~0.2 m in thickness in T2 (ARE), ~1 m in T3 (BAR), and ~0.4-0.5 m in T6 (RUE) and T10 (FON). Pedogenic calcrete formation might follow different paths depending on the local interplay between erosion, deposition and diagenesis (Alonso-Zarza, 2003), occasionally leading to the aerial exposure of the calcrete horizon if erosion overcomes local sedimentation (which is not observed in the studied terraces). As all are soils developed from similar parental materials and in an area of homogeneous climate conditions, assuming a zero-erosion scenario it would be expected that the thickness of the Bk horizon would decrease according to the relative age sequence because the oldest terraces have had more time to developed and have experienced the same climatic variations as those developed at lower levels in the staircase. For instance, the Bk horizon in terrace T2 (ARE) should be at least 0.8 m thicker than it actually is to be similar to that preserved in terrace T3 (closest level placed right below T2). Regarding the location of the Bk horizon in the soils, the upper depth of the Bk horizon in the different terraces is found at ~0.3 m in T2 (ARE), ~0.2 m in T3 (BAR), and ~0.7 m in T6 (RUE) and T10 (FON). Taking as reference both the thickness and the depth of the upper Bk horizon's top in terraces T6 and T10, which show identical values, the oldest terraces T2 and T3 would have experienced a total surface lowering of 1.2 m and 0.5 m respectively. The lowest terraces T11 (SOL) and T12 (ISI) lack a Bk horizon and, hence, the single criteria available are the number and thickness of horizons preserved in the youngest terrace T12. The soil in terrace T12 (ISI) is ~40 cm thicker and better developed (up to three well distinguished horizons) than the soil developed in terrace T11 (SOL) providing a minimum lowering estimate for the latest. Finally, for terraces T6, T10 and T12, a total surface lowering value of 0.2 m has been arbitrarily assumed to avoid an unrealistic null value. The soil-based scenario simplifies factors involved in soil formation (especially at local level, which hampers a soil-based lowering estimation with confidence), but it offers an alternative scenario where total surface lowering since terrace abandonment is minimal instead of zero. The two lowering scenarios showcase well how this parameter affects exposure age interpretation.

4.3. Age model results

The ^{10}Be–^{26}Al concentrations measured in six depth profiles were used to obtain multiple CSEB models for the Duero river terraces (Figure 6) considering different maximum lowering scenarios (Table III). Exposure ages for terraces T3 to T12 would range between 2.5 and 0.14 Ma when no constraint on maximum lowering is applied (only the morpho-stratigraphic order of the terraces was considered; Figure 7). If the maximum lowering is constrained based on geomorphological interpretations and measurements made in topographic sections, resultant exposure ages for the investigated terraces would be: 2265 to 265 ka for T3; 2210 to 478 ka for T6; 1078 to 554 ka for T10; 549 to 117 ka for T11; and 217 to 150 ka for T12. However, exposures ages would be considerably younger when total surface lowering is estimated based on soil characteristics. Assuming a scenario of minimum total surface lowering (up to 0.2 m) for terraces showing well-preserved soils and additional lowering increases for other terraces based on soil observations previously discussed, we obtained: 997 to 284 ka for T3; 611 to 449 ka ka for T6; 325 to 248 ka for T10; 171 to 100 ka for T11; and 142 to 115 ka for T12. The lack of degrees of freedom in the ^{10}Be–^{26}Al model of terrace T2 prevents the calculation of the surface exposure age uncertainty, and hence, results displayed in Table III for the two lowering scenarios proposed would only constitute a minimum estimate.

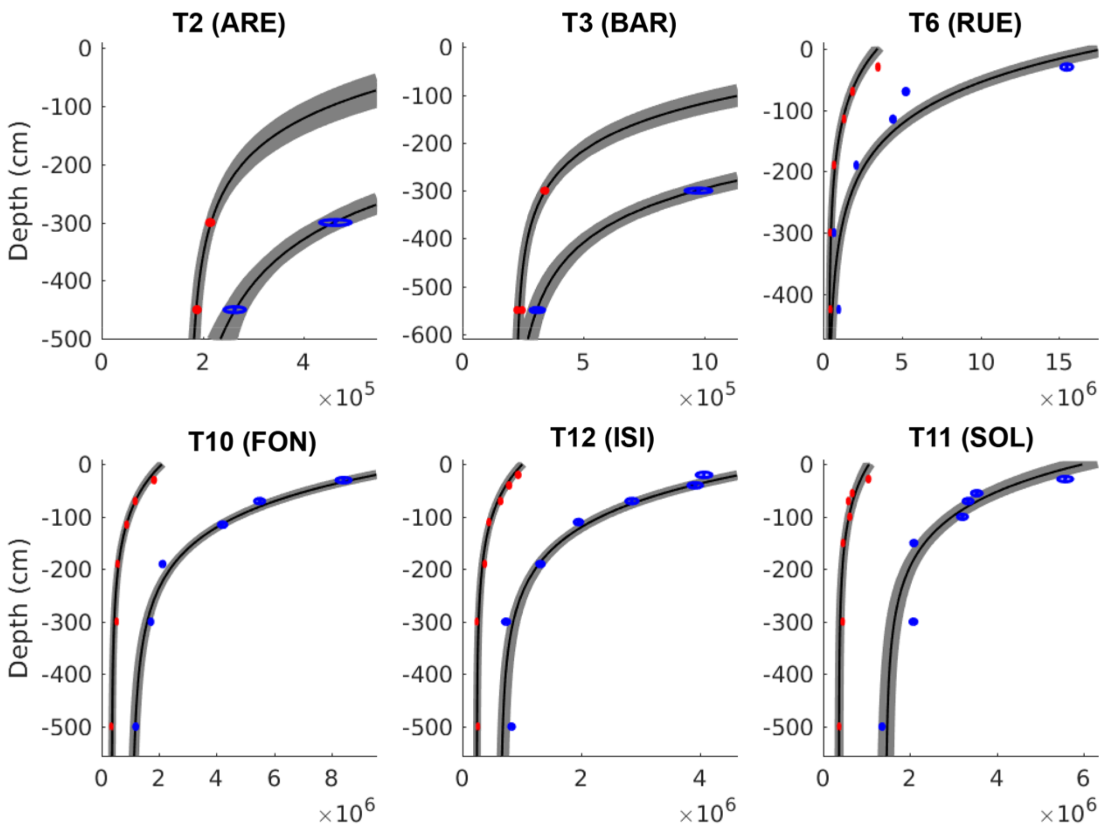

Figure 6.- Best fitting CSEB models (black lines) fitting the ^{10}Be and ^{26}Al concentrations (red and blue ellipses) and CSEB models fitting the data within one-sigma confidence level (grey lines).

Table III.- CSEB dating age models of fluvial terraces sampled upstream from the WCB (sampling locations are shown in Figure 2) considering three different scenarios of maximum lowering: free (lowering limited to 100 m); maximum total lowering estimated from surface preservation; and maximum lowering estimated from soil characteristics. Due to the lack of degrees of freedom in profile adjustment, the exposure ages provided for T2 must be considered only minimum estimates.

Terrace (lowering)	Relative height (m)	^{10}Be inherited (10^4 at.g^{-1})	^{26}Al inherited (10^4 at.g^{-1})	Basin denudation rate (m.Ma^{-1})	Exposure age (Ma)	Burial duration (Ma)	In situ denudation rate (m/Ma)
T2 (free)	+133–128	14.4–17.8	0 –19.6	0–6.3	0.08–∞	3.67–10.10	<16.8
T3 (free)	+112–107	17.8–21.9	0–15.1	0–3.4	0.27–2.50	4.50–9.66	<4.4
T6 (free)	+85–81	30.0–38.9	7.2–37.5	0–3.1	0.50–∞	3.55–7.88	<1.6
T10 (free)	+ 39–34	30.3–33.5	79.3–93.1	8.0–10.7	1.79–∞	1.67–1.97	2.7–3.3
T11 (free)	+26–22	31.2–38.4	117.7–151.3	9.7–14.1	0.13–∞	0.94–1.39	0.5–8.7
T12 (free)	+13–11	22.3–24.8	53.4–69.5	10.4–12.7	0.14–0.73	1.72–2.15	<6.9
T2 (5 m)	+133–128	15.3–17.8	2.3 –19.5	0.8–6.3	0.10–0.91	3.67–7.41	<15.1
T3 (3.5 m)	+112–107	17.8–22.0	0–15.2	0–3.4	0.27–2.27	4.48–9.67	<3.9
T6 (3 m)	+85–81	31.9–38.8	9.6–36.8	0.6–2.6	0.48–2.21	3.80–6.09	<1.6
T10 (3 m)	+ 39–34	32.6–35.5	85.8–103.6	7.6–9.5	0.55–1.08	1.65–1.94	2.7–3.3
T11 (4 m)	+26–22	32.9–38.4	126.7–151.2	9.7–13.4	0.12–0.55	0.92–1.34	<8.4
T12 (1.5 m)	+13–11	23.5–25.1	58.7–67.7	10.4–12.9	0.15–0.22	1.73–2.10	0.6–5.6
T2 (1.4 m)	+133–128	16.4–18.0	11.0 –19.2	3.7–6.2	0.10–0.38	3.70–4.70	<9.9
T3 (0.7 m)	+112–107	19.6–22.0	4.8–15.5	1–3.3	0.28–0.98	4.47–6.53	<1.8
T6 (0.2 m)	+85–81	34.9–39.9	22.0–41.3	1.3–3.1	0.45–0.61	3.53–4.80	<0.4
T10 (0.2 m)	+ 39–34	34.7–37.4	96.3–114.1	7.7–9.4	0.25–0.33	1.54–1.83	<0.7
T11 (0.6 m)	+26–22	34.1–38.4	132.8–152.4	9.7–13.2	0.10–0.17	0.91–1.31	<4.2
T12 (0.2 m)	+13–11	23.5–25.2	60.7–70.1	10.5–12.6	0.12–0.14	1.74–2.03	<1.6

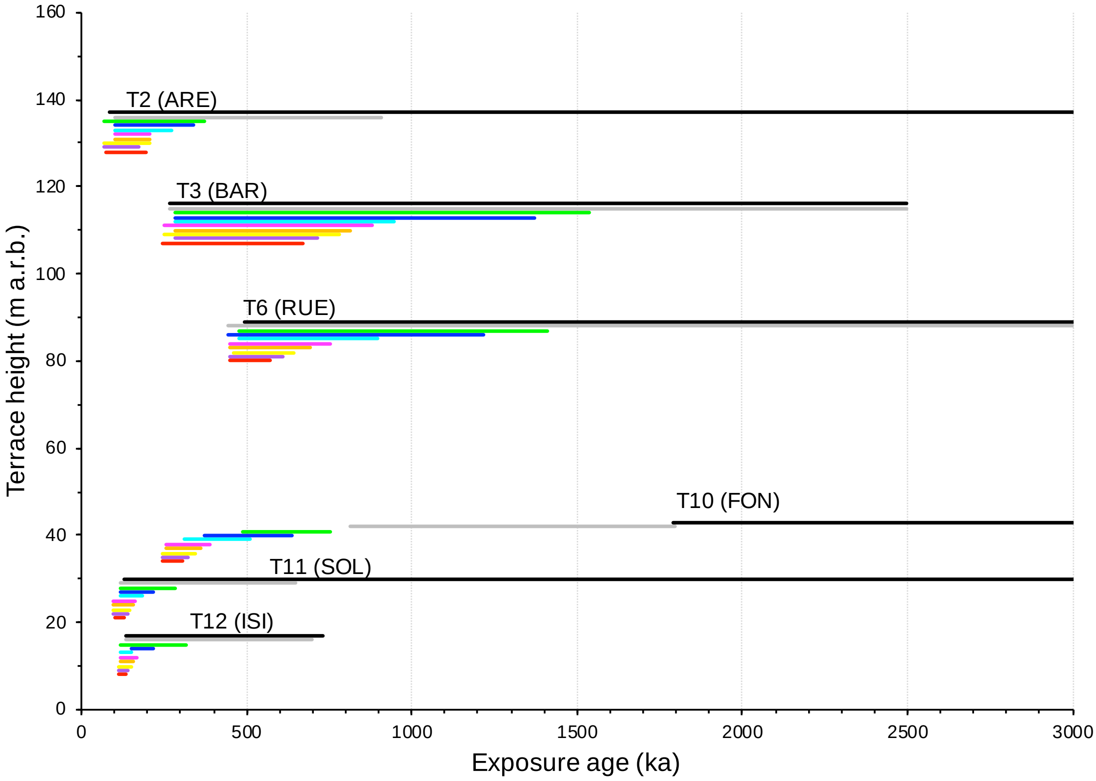

Figure 7.- Exposure ages of CSEB models fitting the data with no restrictions (black) and with limited maximum total lowering of the terrace surfaces by 5 m (grey), 2 m (green), 1.5 m (blue), 1 m (cyan), 0.5

m (magenta), 0.4 m (orange), 0.3 m (yellow), 0.2 m (violet), and 0.1 m (red). Without lowering limitation based on local evidence, the exposure age of most terraces (T3 to T12) is limited to 2.5 Ma based on the maximum exposure age of T3 (ARE).

Burial durations reported for the studied terraces cover the time interval 0.9 to 2.0 Ma for terraces T10 (FON), T11(SOL) and T12 (ISI), while those found in the highest terraces T6 (RUE), T3 (BAR) and T2 (ARE) cover a longer time interval of 3.5 to 9.6 Ma, evidencing longer transport times and complex exposure histories for the highest terraces (Figure 8). Modelled basin denudation rates coetaneous to the oldest terrace levels were much lower (up to 3–6 m·Ma^{-1}) than those found (7.7–13.4 m·Ma^{-1}) in the youngest terraces.

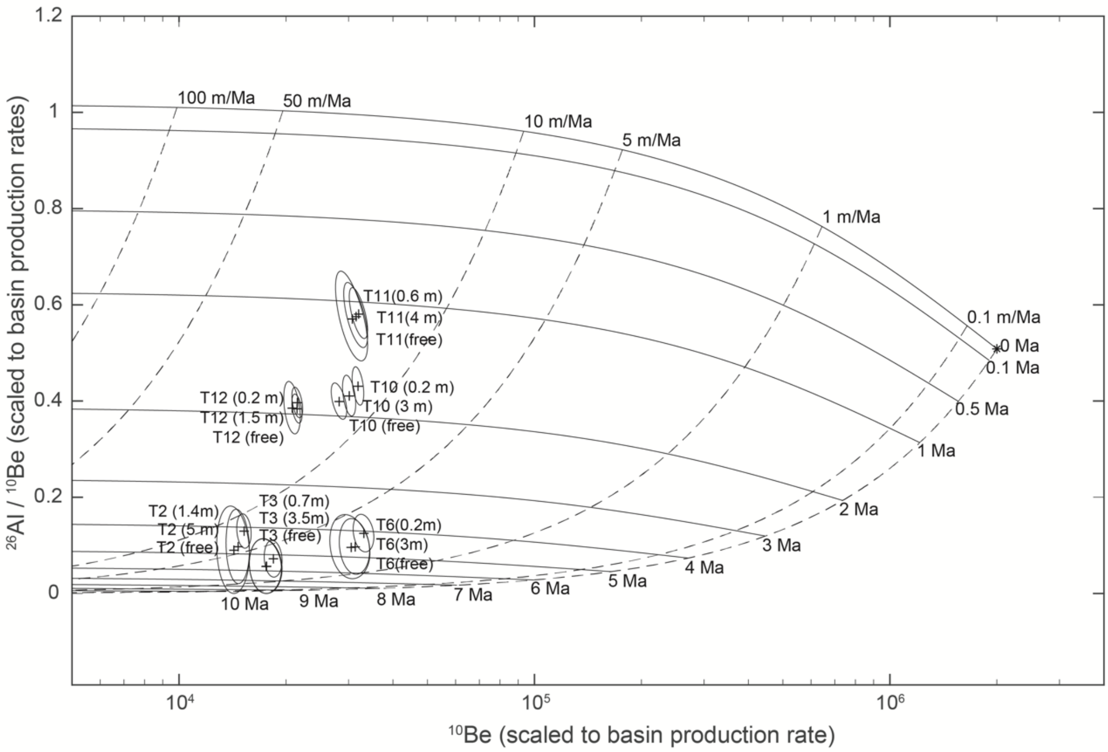

Figure 8.- Inherited concentrations from table III plotted over a “banana plot” generated using the average basin production rates, following Lal & Arnold (1985). The mountain ranges that limit the Cenozoic Duero Basin worked as source area of sediments, located at a mean elevation of 1300 m (estimation based on a 25 m resolution DEM from the Spanish National Institute of Geography). Therefore, all ^{10}Be and ^{26}Al concentrations in this figure are scaled to surface production rates of 11.3 and 76.5 at·g^{-1}·a^{-1} respectively. This model allows us to classify the origin of these sediments in two groups: an old group of sediments found in T2, T3 and T6 generated c. 5 Ma ago at a stable landscape (apparent denudation rate < 10 m·Ma^{-1}); and a young group of sediments found at T10, T11 and T12 generated 2 –1 Ma ago at an active landscape (apparent denudation rate > 10 m·Ma^{-1}).

5. Discussion

5.1.Pattern of erosion at basin scale and timing of basin opening

Calculated exposure time using the CSEB model of Rodés et al. (2014) combined with the terrace staircase configuration (which indicates the relative age sequence) provides a time reference for the starting point of incision and terrace formation as a landform within the landscape (abandonment age). The abandonment age is limited to ca. 2.27–0.55 Ma in terrace T3 (+112–107 m), ca. 2.21–0.55 Ma in terrace T6 (+85–81 m), ca. 1.08–0.55 Ma in terrace T10 (+39–34 m), 0.55–0.15 Ma in terrace T11 (+26–22 m), and 0.22–0.15 Ma in terrace T12 (+13–11 m) for a lowering scenario constrained based on terrace topography and considering the relative age sequence (helps in narrowing the mathematical solutions of the CSEB model incompatible with the staircase configuration). Thus, terraces T3 to T6 would be ascribable to the Early Pleistocene, T10 to the Early-Middle Pleistocene and terraces T11 and T12 to the Middle Pleistocene. In contrast, the abandonment age is limited to ca. 0.98–0.45 Ma in terrace T3 (+112–107 m), ca. 0.61–0.45 Ma in terrace T6 (+85–81 m), ca. 0.33–0.25 Ma in terrace T10 (+39–34 m), 0.17–0.12 Ma in terrace T11 (+26–22 m), and 0.14–0.12 Ma in terrace T12 (+13–11 m) for a lowering scenario constrained based on soil characteristics, ascribing terraces T3 to T6 to the Early-Middle Pleistocene, terrace T10 to the Middle Pleistocene, and terraces T11 and T12 to the Middle-Upper Pleistocene. Both scenarios provide an estimate for the timing of floodplain abandonment and terrace formation due to river incision that seem to be in agreement with previous interpretations, based on other techniques (OSL/TL, AAR, ESR and palaeomagnetic chronologies), which ascribed the full terrace staircase to the Pleistocene (Silva et al., 2017). They are also consistent with previous interpretations based on erosional surfaces developed on top of the Neogene infill sediments at the CDB. Close to the Iberian Chain, the top surface of the UPL shows karstification evidence that has been ascribed to the Late Miocene-Early Pliocene, due to a sedimentation break before the onset of the Neogene basin emptying (Benito-Calvo and Pérez-González, 2007). A second erosional surface (LPS) was formed at a lower elevation, on top of the LPL (Figure 2), which connects with the top surface of alluvial fans close to the source area of sediments in the Iberian Chain (Benito-Calvo and Pérez-González 2007). According to these authors, the LPS was formed prior to Pleistocene fluvial incision and could be considered Pliocene or Plio-Pleistocene. Thereafter, the highest terraces linked to the Duero river (T1, T2 and T3) were formed upstream from the Duero knickzone in the Early Pleistocene, starting at T1, the uppermost terrace preserved (+135–131 m respect the modern floodplain), which locates several tens of meters below the LPS (Figure 2). If the soil-based lowering scenario is considered, the ages obtained for the lowest terraces in our study area (hanging at +39 and +13 m) yield comparable depositional ages to those obtained through OSL by Cunha et al. (2019) in the DLR, which are hanging between +53 and +13 m above the river bed between Pocinho and Barca d'Alva (ca. 360–12 ka). In contrast, the lowest terraces at the DLR are remarkably younger than the lowest terraces in the CDB when the lowering scenario based on terrace surface topography is considered. In any case, the DLR terraces are located downstream the Arribes knickzone at 200 m a.s.l. (500 m below the terrace staircase studied here), and point to several stages of terrace formation in a different stretch of the Duero long profile placed between the Duero lower and upper reaches (DLR and CDB respectively; Figure 1).

The inherited cosmogenic nuclides in a depth profile represent the signature of the sediment at the time of its deposition. In a simple burial history, sediments are eroded from the source area and deposited in a river terrace carrying an inherited cosmogenic signature that is proportional to the average exhumation rate at the source area and the travel time until being buried. However, more complex histories with multiple exhumation/burial episodes before the final burial event are also possible. Presumably, sediments found in the Duero terrace depth profiles come from a diverse source area located at the basin periphery, the highlands of the Cantabrian Mountains to the North, the Iberian Chain to the East and the Sistema Central to the South. Moreover, sediments eroded from the source area might have been mixed with recycled sediments from the Duero Cenozoic Basin, resulting in a material with mixed signature. Thus, inheritance-derived ages and basin erosion rates might inform on the evolution of the basin's bedrock denudation through time, while apparent burial durations may provide an estimate for the maximum travel time of sediments from the source area to the terrace in which they were found. These are key factors potentially related to the landscape response to exorheism.

Apparent burial durations calculated from the inherited ^{10}Be and ^{26}Al concentrations in the highest terraces (T2, T3 and T6) indicate maximum sediment travel times in the range 3.5 to 9.7 Ma, while those found in the lowest terraces (T10, T11 and T12) yield values between 0.9 and 2.2 Ma (Figure 9). The several million-years difference between the maxima and minima values reported for the highest terraces is compatible with higher proportions of recycled sediments with inherited ^{10}Be–^{26}Al concentrations. Also, apparent burial durations in the older terraces seem to be in reverse stratigraphic order, suggesting that the river was eroding a basin filled with sediments from top (younger sediments) to bottom (older sediments) when sediments included in T2 and T3 were formed (>3.5 Ma). Average denudation in the basin source remained relatively low (<3-6 m·Ma^{-1}), suggesting that these palaeo-sediments were generated in a stable and relatively inactive basin.

Sediments included in the lowest terraces (T10, T11 and T12) indicate that average denudation rates at basin scale were already doubled (7.7–13.4 $m{\cdot}Ma^{-1}$) ~2–1 Ma ago. The lower proportion of inherited sediments and the acceleration of denudation rates at basin scale are both reflecting that sediments included in the lowest terraces contain a higher proportion of fresh sediments eroded from bedrock than those found in the highest terraces (Figure 9). A moderate mixed origin of sediments is then assumed for the lowest terraces possibly generated as the upper Duero River started to cut through bedrock materials under much more erosive conditions, with basin average denudation rates comparable to those found in other exorheic basins across Europe (e.g. Schaller et al., 2016a).

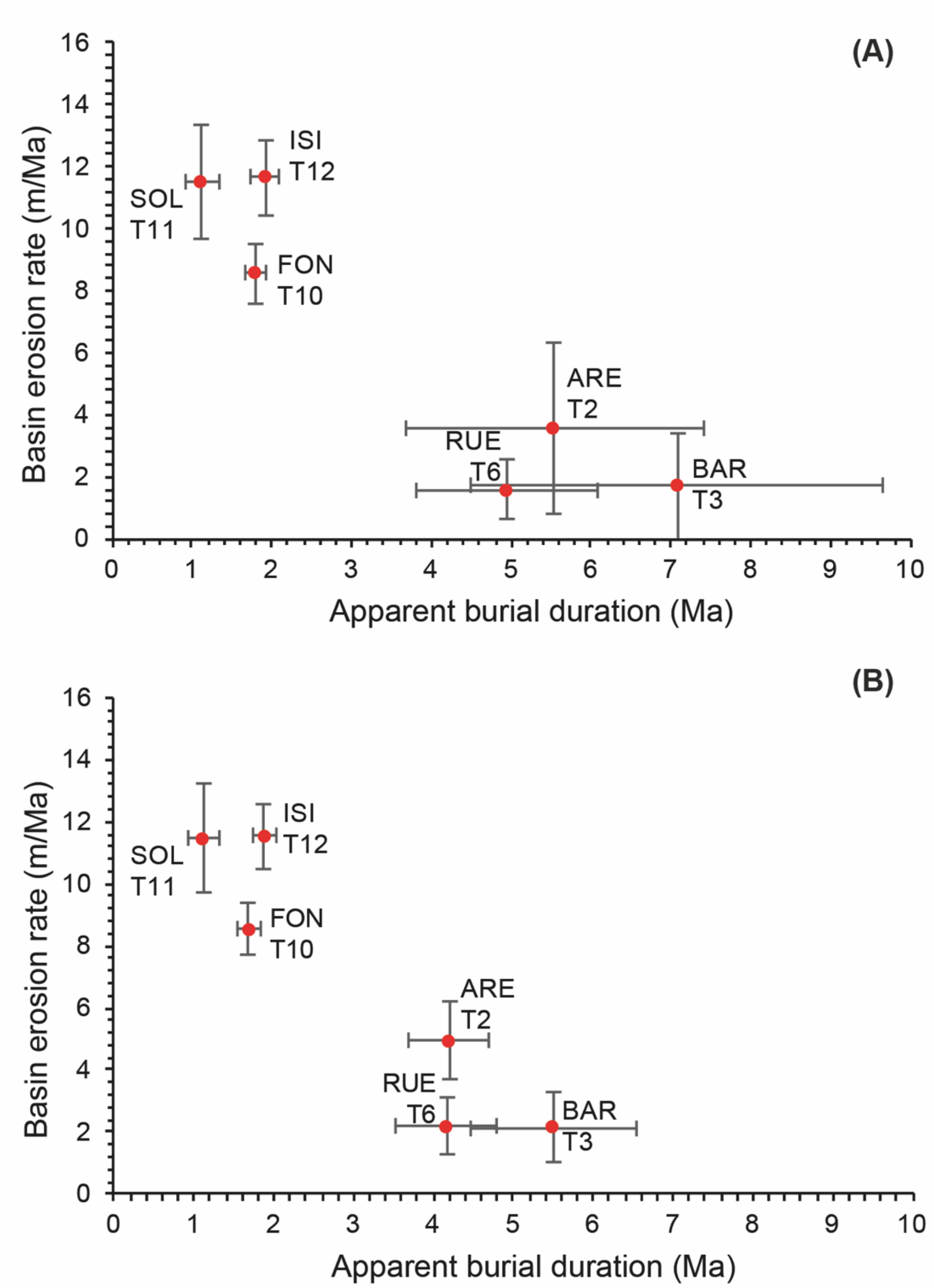

Figure 9.- Apparent basin denudation rates in the catchment area (y-axis) and apparent burial durations (x-axis) are both calculated from inherited ^{10}Be –^{26}Al concentrations measured in the terrace depth profiles. They are both representative for the Duero Basin evolution and the exposure history of sediment particles until being deposited in the studied terraces: (A) maximum lowering constrained based on terrace surface topography and (B) maximum lowering constrained based on soil characteristics. In both lowering scenarios, the highest terraces indicate lower basin denudation rates and older apparent burial durations than in the lowest terraces, reflecting a considerable acceleration of incision along the upper Duero river around 2 Ma, already in response to the basin opening to the Atlantic Ocean.

The opening of a closed basin involves a change in the long profile of the drainage network as the incision wave migrates upstream from the opening point. The acceleration of the basin denudation rates around ca. 4–2 Ma, and the marked differences in the inherited signatures of the terrace deposits, evidence a timing delay between the basin opening and the arrival of the retrogressive erosive wave, nucleated at the opening zone, to the source area of sediments. This delay supports the hypothesis of the two trains of knickpoint waves traveling at different speeds through the soft Neogene sediment cover and the hard-Paleozoic bedrock (Struth et al., 2019). Hence, the low-propagating knickpoint wave travelling through the more resistant Paleozoic bedrock in the WCB basin likely regulates how fast the incision wave is transmitted upstream, while the terrace staircase formation across the basin will mostly respond to the fast-propagating waves that travel through the soft Neogene sediment cover.

Regarding the timing of the basin opening, compared to other Cenozoic basins from the Iberian Peninsula, the endo-exhoreic transition of the Duero Basin is likely to have occurred after that of the Ebro Basin (Antón et al., 2019). In the Ebro Basin, the fluvial network attained an advanced phase of adjustment since the opening of the foreland basin towards the Mediterranean Sea (Soria-Jáuregui et al., 2019). Resultant fluvial incision was able to induce as much as 630 m of uplift due to isostatic rebound, which is consistent with an opening age of 12.0–7.5 Ma obtained restoring the flexural isostatic compensation linked to infill erosion (García-Castellanos and Cruz-Larrasoaña, 2015). In contrast, the Duero Neogene infill is poorly dissected and it pretty much preserves the pre-opening topography, with an estimated average surface lowering limited to 65 ± 13 m (Antón et al., 2019). Besides, the Duero river profile remains in disequilibrium illustrating a transient erosive response to the opening (Antón et al., 2014). The comparative analysis of chi-indices and knickpoint distribution for both basins highlights these differences, and the recalculated chi values once the drainage area is removed also supports the hypothesis of a recent endo-exorheic transition of the Duero Basin (Struth et al., 2019). Hence, a basin opening towards the Atlantic Ocean later than ca. 4-5 Ma, derived from our data, agrees with previous interpretations that assume a Plio-Pleistocene age for the basin switching from sedimentation to erosion due to its opening into the Atlantic Ocean (Benito-Calvo and Pérez-González, 2007; Silva et al., 2017; Antón et al., 2019; Cunha et al., 2019).

5.2.Spatial variation of fluvial incision and denudation rates

The CSEB model suggests that the erosive fingerprint of the basin endo-exorheic transition was important at the source area of sediments since at least 2–1 Ma ago, marked by the increase in apparent basin denudation rates and the increased proportion of fresh sediments recorded in the lowest terraces. This interpretation is consistent with Electro Spin Resonance (ESR) chronologies reported for fluvial terraces in the Arlanzón and Arlanza valleys, two tributaries of the Duero river placed more than 130 km upstream from our study area (Table IV and Figure 10). In the Arlanzón River an ESR age of 1.14 ± 0.13 Ma was reported for terrace T3 (+78–70 m), while the inferior levels provided the following results (Moreno et al., 2012): (i) 0.78 ± 0.12 and 0.93 ± 0.10 Ma for terrace T4 (+67–60 m); (ii) 0.70 ± 0.10 Ma for terrace T5 (+54–50 m); (iii) 0.40 ± 0.09 Ma for terrace T8 (+35–26 m); and (iv) 0.14 ± 0.02 Ma for terrace T11 (+13–12 m). Similarly, the ESR chronology of the nearby Arlanza River yielded ages of 0.79 ± 0.11 Ma for terrace T5 (+79–73 m); 0.70 ± 0.07 Ma for terrace T6 (+67–64 m); 0.35 ± 0.04 Ma for terrace T10 (+36–33 m); and 0.23 ± 0.03 Ma for terrace T12 (+23–20 m), suggesting similar fluvial evolution in both tributaries (Moreno et al., 2016) (Table IV, Figure 10). In the Esla River, a tributary which converges with the Duero river ~50 km downstream from the study area, thirteen terrace levels were described with the highest terrace located at +160 m (Torrent, 1976). Upper terraces are associated to a Paleo-Esla, which switched its course to the west between ∼0.52 Ma and 0.15 Ma (Schaller et al., 2016b). An age of ~1.04 Ma was assigned to the highest level by previous authors, while cosmogenic nuclides analysis in lower fluvial terraces yielded depositional ages of ~0.52 ± 0.20 Ma for the youngest Paleo-Esla terrace at +78–76 m and 0.16 to 0.08 Ma for the lowest Esla terraces at +64–32 m to +8–7 m (Schaller et al., 2016b) (Table IV and Figure 10). Both datasets support the idea that in the tributary valleys close to the source area of sediments most terraces formed over the last ∼1.5–1 Ma, while in our study area the studied terraces were most likely formed since 2.5–1 Ma (depending on the total surface lowering scenario assumed).

Table IV.- Available chronological framework for the Duero fluvial network upstream the Arribes knickzone, including the Arlanzón, Arlanza and Esla tributaries. Incision rate estimations along the main channel for each of these rivers considering available terraces ages and maximum total incision observed for each terrace level at the specific sampling site. Terrace level names according to the references.

Valley	Terrace level	Terrace height (m)	Age (Ma) min	Age (Ma) max	Incision rate (m/Ma) max	Incision rate (m/Ma) min	Reference
Arlanzón	T3	+78-70	1.01	1.27	77	61	Moreno et al. (2012)
	T4	+67-60	0.66	0.9	102	74	
		+67-60	0.83	1.03	81	65	
	T5	+54-50	0.6	0.8	90	68	
		+54-50	0.63	0.77	86	70	
		+54-50	0.49	0.67	110	81	
	T8	+35-26	0.28	0.44	125	80	
		+35-26	0.31	0.49	113	71	
	T11	+13-12	0.12	0.16	108	81	
Arlanza	T5	+79-73	0.68	0.9	116	88	Moreno et al. (2016)
	T6	+67-64	0.63	0.77	106	87	
	T10	+36-33	0.31	0.39	116	92	
	T12	+23-20	0.2	0.26	115	88	
Duero	T3 (3.5 m)*	+112-107	>0.55	2.27	<202	49	This study
	T6 (3 m)*	+85-81	>0.55	2.21	<153	38	
	T10 (3 m)*	+39-34	0.55	1.08	70	36	
	T11 (4 m)*	+26-22	>0.15	0.55	<173	47	
	T12 (1.5 m)*	+13-11	0.15	0.22	87	60	
	T3 (0.7 m)*	+112-107	>0.45	0.98	<249	115	
	T6 (0.2 m)*	+85-81	0.45	0.61	189	139	
	T10 (0.2 m)*	+39-34	0.25	0.33	157	120	
	T11 (0.6 m)*	+26-22	>0.12	0.17	<226	152	
	T12 (0.2 m)*	+13-11	0.12	0.14	113	92	
Paleo-Esla	G; f	+100-95	0.51	0.97	196	103	Schaller et al. (2016b)
	SK; h	+78-76	0.32	0.72	244	108	
		+78-76	0.39	0.72	200	108	
Esla	P; j	+32	0.12	0.24	267	133	
	T20; l	+22-20	0.12	0.24	183	92	
	n	+8-7	0.07	0.12	114	67	

(*) Maximum lowering scenario considered for each terrace surface in the exposure age calculation is provided in brackets.

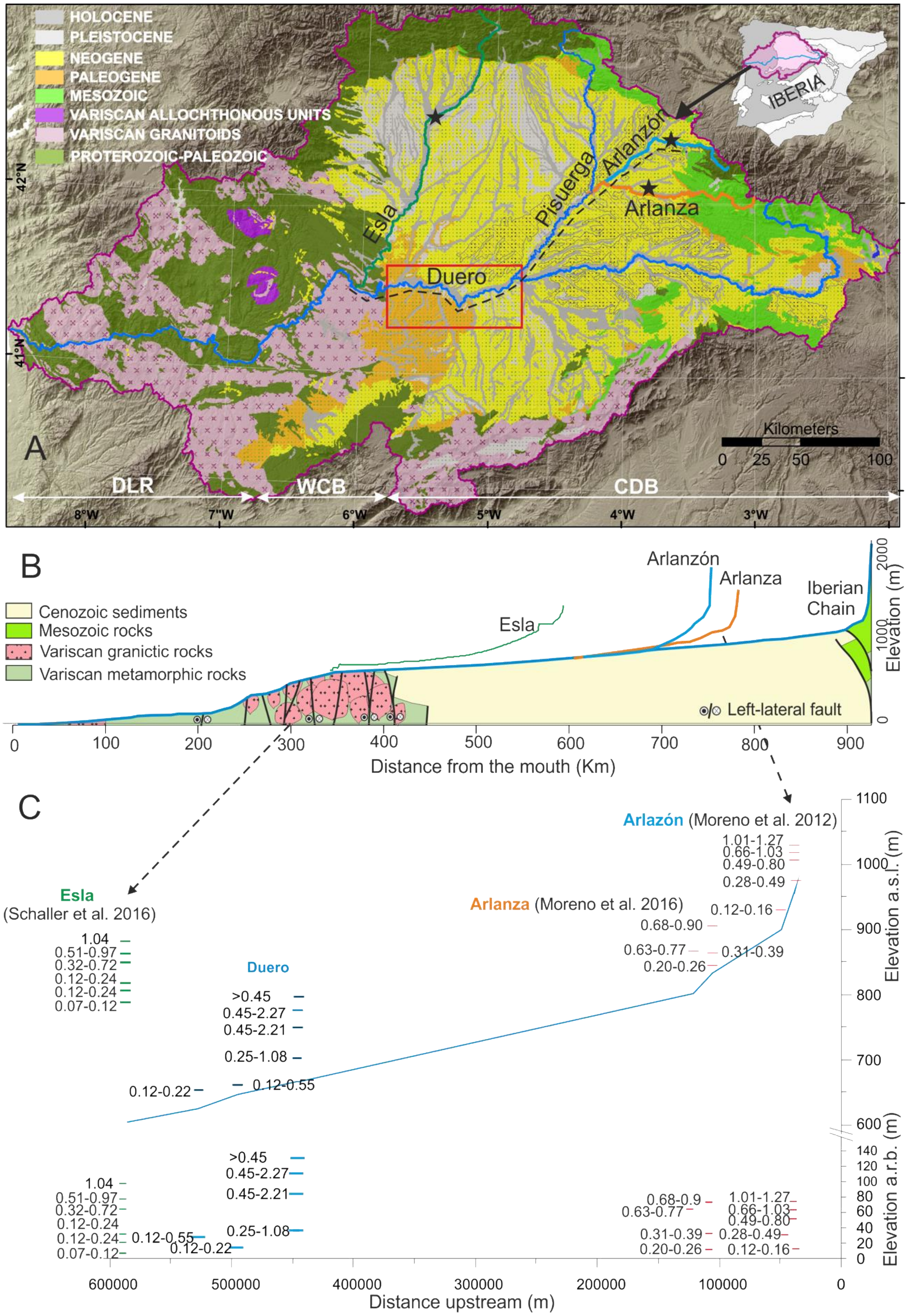

Figure 10.- Synthesis of available chronological data on fluvial terraces for the Duero river and its tributaries: (A) location of dated terrace sequences in the context of the CDB (the rectangle marks the study area; stars indicate the location of other terrace sequences previously dated along the Esla, Arlanza and Arlanzón streams). (B) Long profile of the Duero river and the tributaries with chronological data on terrace sequences (Esla, Arlanza, Arlanzón). (C) Distribution and age (expressed in Ma) of terraces above

the river bed and at their position and elevation over the long profile integrating the Duero and the its tributaries upstream from the WCB up to the Arlanzón. Dashed line in A and arrows in B, show the stretch represented in the integrated long profiles. Chronological data on the Esla river are represented at its confluence's location with the Duero river.

River incision rates were estimated in the study area using the maximum relative height of dated terrace levels as a reference for total incision (up to +112 m) and terrace abandonment ages derived from the CSEB dating model (Table IV). Depending on the lowering scenario considered (Figure 11), time-averaged incision rates deduced from linear adjustment of dated terrace values would range between ca. 43–141 $m \cdot Ma^{-1}$ since 2.3 Ma (lowering scenario #1), or 122–209 $m \cdot Ma^{-1}$ since 1 Ma (lowering scenario #2). These time-averaged incision values obtained close to the basin opening/overspill point seem in turn in agreement with the values obtained upstream. Close to the source area in the Iberian Chain, total incision along the Arlanzón and Arlanza tributaries attained up to 79–78 m over the last 1Ma, involving time-averaged incision rates in the order of 68–88 $m \cdot Ma^{-1}$ and 88–112 $m \cdot Ma^{-1}$, respectively (Figure 11). In contrast, the Esla River attained a total incision up to 100 m for the same period of time as reported by Schaller et al. (2016a), involving time averaged incision rates in the range 105–207 $m \cdot Ma^{-1}$ over the last 1 Ma, which are comparable or slightly lower than those obtained in our study area using the soil-based lowering scenario. These results support the diachronous character of terraces formed through knickpoint propagation as demonstrated in other studies (e.g. Stokes et al., 2002; Rixhon et al., 2011; Baynes et al., 2015; Finnegan, 2013). However, the chronological data on time transgressive formation of terraces and basin denudation in the Duero catchment allow further interpretations to understand general-patterns and rates of landscape adjustment associated to basin scale endo-exorheic transitions.

Table V. - Summary of denudation rates and time-averaged incision rates in the Duero, Esla, Arlanza and Arlanzón sites (compiled in Table IV) considering different time periods. Lowering scenarios in the Duero River are based on terrace surface topography (1) and soils (2).

Time	Duero (scenario 1)	Duero (scenario 2)	Esla	Arlanza	Arlanzón
>3.5 Ma	Basin denudation rates <6 m/Ma (based on inherited ^{10}Be and ^{26}Al from terraces T2, T3 and T6)		Possibly low basin average denudation rates (based on high ^{10}Be inheritances between 0.14 and 0.3 M atoms/g from terraces in Schaller et al., 2016a)	Possibly slow basin denudation rates, as Arlanza and Arlanzón are inside the catchment of T2, T3, T6, T10, T11 and T12.	
Since 2-1Ma	Basin denudation rates rose between 8 and 13 m/Ma (based on inherited ^{10}Be and ^{26}Al from terraces T10, T11 and T12)				
	Incision rates between 36-49 to <202 m/Ma (based on maximum ^{10}Be and ^{26}Al deposition ages of T3, T6 and T10)	—			
Since 1-0.6Ma	Incision rates of 36-70 m/Ma (based on ^{10}Be and ^{26}Al deposition ages of T10)	Incision rates of 115-<249 m/Ma (based on ^{10}Be and ^{26}Al deposition ages of T3)	Incision rates of 103-196 m/Ma based on terrace ^{10}Be deposition ages of paleo-Esla terraces (Schaller et al., 2016b).	Incision rates c. 87-116 m/Ma based on ESR age of terraces T5 and T6 (Moreno et al., 2016)	Incision rates c. 61-102 m/Ma based on ESR ages of terraces T3, T4 and T5 (Moreno et al., 2012)
Since 0.6-0.2 Ma	Incision rates of <173 m/Ma (based on ^{10}Be and ^{26}Al deposition ages of T11)	Incision rates of 120-189 m/Ma (based on ^{10}Be and ^{26}Al deposition ages of T6 and T10)	Incision rates c.108-200 m/Ma (based on terrace ^{10}Be deposition ages in Schaller et al., 2016b). Basin denudation of 60-56 m/Ma (Schaller et al., 2016b)	Incision rates of 88-116 m/Ma based on ESR age of +64m terraces (Moreno et al., 2016)	Incision rates up to 125 m/Ma based on ESR ages of terraces T5, and T8 (Moreno et al., 2012)
Since <0.2 Ma	Incision rates of 60-87 m/Ma (based on ^{10}Be and ^{26}Al minimum deposition age of T12)	Incision rates of ca. 92 to <226 m/Ma (based on ^{10}Be and ^{26}Al minimum deposition age of T11 and T12)	Incision rates between 67 and 114 m/Ma based on ^{10}Be deposition age of terrace 12ESL007 (Schaller et al., 2016b). Basin denudation rates of 33-56 m/Ma (Schaller et al., 2016a)	—	Incision rate of 81-108 m/Ma based on ESR age of terrace T11 (Moreno et al., 2012)

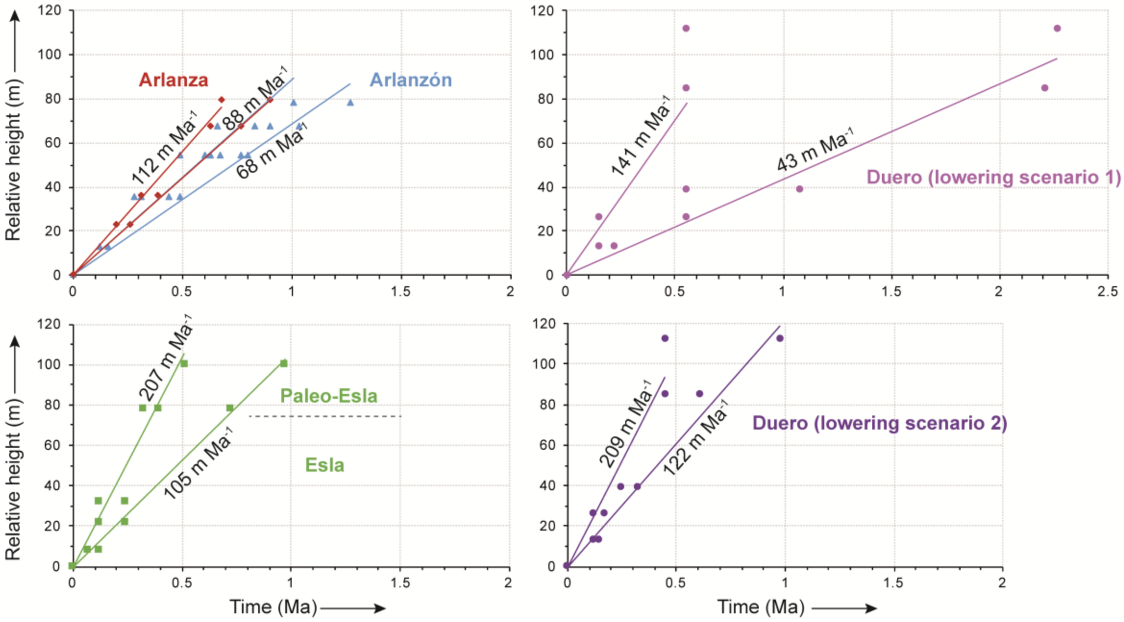

Figure 11.- Comparison between terrace sequences preserved at specific sampling sites along the Arlanzón, Arlanza and Esla tributaries with that recorded along the main Duero river in our study area,

based on datasets compiled in Table V. For the Duero river, the two different lowering scenarios discussed in the main text are provided, which are based on terrace surface topography (1) and soil characteristics (2). Each pair of regression lines represent average incision rates at each site in the basin using the full dataset locally available.

Cyclic fluvial aggradation and entrenchment episodes are frequently interpreted as the response to sustained base-level lowering driven by a combination of tectonic and/or climatic fluctuations (e.g. Bridgland and Westaway, 2008; Cunha et al. 2008). The Duero Basin occupies a relatively stable tectonic setting where evidence of significant tectonic uplift since the late Miocene is absent (De Vicente and Vegas, 2009; Antón et al., 2010). Chronological data on fluvial terraces do not favor a straightforward interplay between climate and terrace formation. Nevertheless, the base level lowering associated at the basin opening seems the main mechanism linked to basin infill dissection and terrace staircase development. In a similar context, Bartz (2019) rule out climate as the main driver mechanism for fluvial aggradation in the Triffa basin (NE Morocco), suggesting that basin scale capture events might dominate a fluvial transient response. Previous works (e.g. Paola et al., 1992; Beaumont et al., 2000), indicate that each system has an intrinsic time response to recover the equilibrium after a climatic perturbation or a change in drainage connectivity. This time is scale-dependent but falls often in the order of millions of years (Whipple and Tucker, 1999; Pazzaglia, 2003, Whipple, 2001; García-Castellanos and Larrasoaña, 2015). Even for much smaller basins of 10 and 70 km^2 in Hatay Graben (Turkey) and the Apennines, Whittaker and Boulton (2012) estimate a fluvial response time in the order of 3–1 Ma. In the Duero river case, the configuration of the crystalline hard bedrock at the WCB might have contributed in delaying the time needed to recover a steady-state profile.

The recorded eastward progression of the incision wave generated in the opening area (Table VI), illustrates the erosional pattern expected in continental basins that underwent an endorheic to exorheic transition, (e.g. Antón et al., 2019; Bartz, 2019; Mather, 2000; Stokes et al., 2002, 2018; Soria-Jáuregui et al., 2019). A strong coupling between the rate of fluvial downcutting and orbital-forcing has been suggested for the Tagus and the Duero rivers, particularly since the establishment of the 100 ka eccentricity cycles (Silva et al., 2017). Our chronological results favor an increase of apparent basin denudation since ~2 Ma, but do not allow an accurate interpretation of the interplays between climate and terrace formation. We assume that changes in sediment supply related to climate cyclicity are superimposed onto the long-term base level lowering, which dominates the fluvial entrenchment in the area. The base level drop resulting from the onset of exorheism generates knickpoint wave trains propagating upstream along the drainage system (Struth et al., 2019). In the Duero, immediately downstream of the study area, the incision is limited by the resistant lithology at the Arribes gorge (WCB, Figure 10), which regulates the transmission of successive knickpoint waves upstream. As the Duero attains incision at the basin outlet (WCB), the erosive wave propagates towards the basin center increasing the profile gradient. While the knickpoint progresses upstream, the fluvial system aggrades downstream to progressively balance the channel gradient. Successive incision waves, due to progressive incision at the basin outlet, will result in fluvial downcutting with the development of the inset Pleistocene river terrace sequence at the basin center and the propagation of the erosional signal along the tributary network to the catchment divide. This model is consistent with an enhanced erosion in the Esla catchment allowing higher incision rates and total incision (highest terrace at +100 m) than in the Arlanza-Arlanzón system placed further upstream (highest terrace ~80 m; Figures 10 and 11). Also, significant differences in terrace patterns and landscape dissection are observed in the main trunk (Rodríguez-Rodríguez et al., 2020), with the highest terraces only preserved upstream at the basin center (Figure 2). At a basin scale, the relatively low average denudation rates derived from the upper terraces are consistent with a null or scarce transmission of the erosive wave nucleated at the opening site along the catchment at that stage. In contrast, by the time of the lowest terraces formation (T10, T11 and T12) denudation rates doubled, suggesting the establishment of much more erosive conditions at basin scale and the arrival of the enhanced erosional signal to the basin source.

The Cenozoic Duero basin is an exceptional example to understand the evolution of sedimentary basins and longer-term landscape response associated to a continental scale drainage reorganization. Results provide a chronological framework for the terrace sequence and illustrate the main role of autogenic mechanisms in landscape dissection and terrace staircase formation in response to basin-scale endorheic to exorheic drainage transition.

6. Conclusions

Paired ^{10}Be–^{26}Al concentrations measured in six terrace depth profiles of the Duero fluvial terrace staircase upstream from the western margin of the Cenozoic basin provide important insights about the timing of the endo-exorheic transition and subsequent basin evolution:

1) Inherited ^{10}Be–^{26}Al concentrations suggest an increase in basin denudation rates after the basin opening to the Atlantic Ocean. Basin average denudation rates remained relatively low (<3–6 m·Ma^{-1}) until at least 3.5 Ma, showing higher proportions of recycled sediments, and then experienced an acceleration at ca. 2–1 Ma (8–13 m·Ma^{-1}).
2) Terrace surface exposure ages obtained with the CSEB model can be constrained by limiting the total amount of surface lowering based on geomorphic and soil indicators. Future studies based on alternative dating methods might help to better constrain the most probable post-depositional lowering scenario for the studied terraces. In any case, the CSEB model favors Pleistocene ages (<2.5 Ma) for the terraces belonging to the Duero staircase.
3) The apparent change in basin-scale denudation rates is in agreement with the propagation of an eastward erosive wave through the study area as proposed by Struth et al. (2019), nucleated at the western fringe of the basin during the endo-exorheic transition. This wave might have arrived at the basin source between ~1 to 2 Ma ago, being T10 the oldest terrace clearly containing sediments that record the starting of the upper Duero incision in bedrock. This is consistent with previous chronologies reported for some of the oldest terraces preserved in tributary rivers like the Arlanzón, Arlanza and Esla, where the oldest terrace ages are around 1 Ma.
4) Time-averaged incision rates over the last million years display the highest values close to the opening site of the CDB (122 to <250 m·Ma^{-1} in the Duero River; 105–207 m·Ma^{-1} in the Esla River), and the lowest values close to the eastern boundary of the catchment (68–88 m·Ma^{-1} in the Arlanzón River).

Altogether, these findings support the diachronous character of landscape dissection through knickpoint propagation from the opening zone and illustrate the time transgressive formation of terraces along the Duero catchment.

Acknowledgements

This is a MITE contribution (Spanish Government *Plan Estatal de Investigación Científica y Técnica y de Innovación*, CGL2014-59516 & PR2011-0044). At the time of paper writing, L. Rodríguez-Rodríguez was recipient of an outgoing post-doctoral grant of the Clarín-Cofund program (Ref. ACA-17-19), financed jointly by the regional government of Principality of Asturias and the 7th WP of the European Union–Marie

Curie Actions. The ASTER AMS national facility (CEREGE, Aix en Provence) is supported by the INSU/CNRS, the ANR through the "Projets thématiques d'excellence" program for the "Equipements d'excellence" ASTER-CEREGE action and IRD. Candela Pastor-Martín is thanked for the GIS technical support (funded under grant PEJ-2014-A-93258). We thank Martin Stokes and Zsófia Ruszkiczay-Rüdiger for their constructive reviews on the manuscript, which helped us to improve the initial version. We are also thankful to the enterprises Arentis Aridos S.L., Barbado Martín S.L., Aridos Sola e Hijos S.L., and Jose Isidro Torres S.L. for allowing us to sample fluvial sediments in exposed terrace sections at their exploitation quarries.

References

Alonso, J.L., Pulgar, J.A., García-Ramos, J.C., Barba, P., 1996. Tertiary basins and Alpine tectonics in the Cantabrian Mountains (NW Spain). In: Friend, P.F., Dabrio, C.J. (Eds.), Tertiary Basins of Spain: the stratigraphic record of crustal kinematics. Cambridge University Press, Cambridge, pp. 214–227.

Alonso-Gavilán, G., Armenteros, I., Carballeira, J., Corrochano, A., Huerta, P., Rodríguez, J., 2004. Cuenca del Duero. In: Vera, J.A. (Ed.), Geología de España. IGME, Madrid, pp- 550-556.

Alonso Gavilan, G., Dabrio, C.J., Mediavilla, R.M., Armenteros, I., 1989. Procesos sedimentarios y desarrollo de Sand Flats en ríos arenosos del Eoceno del suroeste de la depresion del Duero. Studia Geologica Salmanticensia, Extraordinario No. 5, 159-176.

Alonso-Zarza, A.M., 2003. Palaeoenvironmental significance of palustrine carbonates and calcretes in the geological record. Earth-Science Reviews 60, 261-298.

Alonso-Zarza, A.M., Armenteros, I., Braga, J.C., Munoz, A., Pujalte, V., Ramos, E., Aguirre, J., Alonso Gavilan, G., Arenas, C., Baceta, J.I., Carballeira, J., Calvo, J.P., Corrochano, A., Fornos, J.J., Gonzalez, A., Luzon, A., Martin, J.M., Pardo, G., Payros, A., Perez, A., Pomar, L., Rodriguez, J.M., Villena, J., 2002. Tertiary. In: W. Gibbons, T. Moreno (Eds.), The geology of Spain. Geological Society, Bath, United Kingdom, pp. 293-334.

Antón, L., Muñoz-Martín, A., De Vicente, G., 2010. Alpine paleostress reconstructions and active faulting in Western Iberia. Central European Journal of Geosciences 2, 152-164.

Antón, L., De Vicente, G., Muñoz-Martín, A., Stokes, M., 2014. Using river long profiles and geomorphic indices to evaluate the geomorphological signature of continental scale drainage capture, Duero basin (NW Iberia). Geomorphology 206, 250-261.

Antón, L., Muñoz-Martín, A., De Vicente, G., 2019. Quantifying the erosional impact of a continental scale drainage capture in the Duero Basin (NW Iberia). Quaternary Research, 91(2), 457-471.

Antón, L., Rodés, A., De Vicente, G., Pallàs, R., Garcia-Castellanos, D., Stuart, F.M., Braucher, R., Bourlès, D., 2012. Quantification of fluvial incision in the Duero Basin (NW Iberia) from longitudinal profile analysis and terrestrial cosmogenic nuclide concentrations. Geomorphology, 165–166, 50-61.

Arnold, M., Merchel, S., Bourlès, D., Braucher, R., Benedetti, L., Finkel, R.C., Aumaître, G., Gottdang, A., Klein, M., 2010. The French accelerator mass spectrometry facility ASTER: Improved performance and developments. Nuclear Instruments and Methods in Physics Research B, 268, 1954-1959.

Balco, G., 2017. Production rate calculations for cosmic-ray-muon-produced ^{10}Be and ^{26}Al benchmarked against geological calibration data. Quaternary Geochronology 39, 150-173.

Balco, G., Stone, J.O., Lifton, N.A., Dunai, T.J., 2008. A complete and easily accessible means of calculating surface exposure ages or erosion rates from ^{10}Be and ^{26}Al measurements. Quaternary Geochronology, 3 (3), 174-195.

Bartz, M., 2019. Quaternary fluvial environments in NE Morocco inferred from geochronological and sedimentological investigations. E&G Quaternary Science Journal 68, 1-4.

Baynes, E.R.C., Attal, M., Niedermann, S., Kirstein, L.A., Dugmore, A.J., Naylor, M., 2015. Erosion during extreme flood events dominates Holocene canyon evolution in northeast Iceland. Proceedings of the National Academy of Sciences, 112 (8), 2355-2360.

Beamoud, E., Garcés, M., Montes, M., Nozal, F., Calvo, J. P., López-Olmedio, F., Luengo, J., 2006. Magnetoestratigrafía del Mioceno de las cuencas del Tajo y del Duero. Proceedings of the IV Simposio de Paleomagnetismo Ibérico (MAGIBER), vol. 4, pp. 9-12.

Beaumont, C., Kooi, H., Willett, S., 2000. Coupled tectonic-surface process models with applications to rifted margins and collisional orogens. In: Summerfield, M.A. (Ed.), Geomorphology and Global Tectonics. Chirchester, John Wiley and Sons, pp. 28–55.

Benito-Calvo, A., Pérez-González, A., 2007. Erosion surfaces and Neogene landscape evolution in the NE Duero Basin (north-central Spain). Geomorphology 88, 226-241.

Benito-Calvo, A., Pérez-González, A. y Pares, J.M., 2008. Quantitative Reconstruction of Late Cenozoic Landscapes: A Case Study in the Sierra de Atapuerca (Burgos, Spain). Earth Surface Processes and Landforms 33 (2), 196-208.

Braucher, R., Merchel, S., Borgomano, J., Bourlès, D., 2011. Production of cosmogenic radionuclides at great depth: A multi element approach. Earth and Planetary Science Letters 309 (1-2), 1-9.

Bridgland, D.R., Westaway, R., 2008. Preservation patterns of Late Cenozoic fluvial deposits and their implications: Results from IGCP 449. Quaternary International 189, 5-38.

Capote, R., Insua Arévalo, J.M., Martínez-Díaz, J.J., Martín-González, F., Tsige, M., 2002. La Sierra de Cártama: Pliegue con actividad reciente en las Béticas Occidentales (Hoya de Málaga). Geogaceta 31, 135–138.

Cunha, P., Martins, A.A., Huot, S., Murray, A., Raposo, L., 2008. Dating the Tejo river lower terraces in the Rodao area (Portugal) to assess the role of tectonics and uplift. Geomorphology 64, 271-298.

Cunha, P., Martins, A.A., Gomes, A., Stokes, M., Cabral, J., Lopes, F.C., Pereira, D., de Vicente, G., Builaert, J.P., Murray, A.S., Antón, L., 2019. Mechanism and age estimates of continental-scale endorheic to exorheic drainage transition: Douro River, Western Iberia. Global and Planetary Change 181, https://doi.org/10.1016/j.gloplacha.2019.102985

Chmeleff, J., von Blanckenburg, F., Kossert, K., Jakob, D., 2010. Determination of the ^{10}Be half-life by multicollector ICP-MS and liquid scintillation counting. Nuclear Instruments and Methods in Physics Research Section B: Beam Interactions with Materials and Atoms, 268 (2), 192-199.

Demoulin, A., Mather, A., Whittaker, A., 2017. Fluvial archives, a valuable record of vertical crustal deformation. Quaternary Science Reviews 166, 10-37.

De Vicente, G., Vegas, R., 2009. Large-scale distributed deformation controlled topography along the western Africa-Eurasia limit: Tectonic constraints. Tectonophysics 474 (1-2), 124-143.

Dunai, T.J., 2010. Cosmogenic Nuclides: Principles, concepts and applications in the Earth Surface Sciences. Cambridge University Press, 187 pp.

Finnegan, N.J., 2013. Interpretation and downstream correlation of bedrock river terrace treads created from propagating knickpoints. Journal of Geophysical Research: Earth Surface, 118 (1), 54-64.

Friend, P.F., Dabrio, C.J., 1996. Tertiary basins of Spain: the stratigraphic record of crustal kinematics. Cambridge University Press, Cambridge.

García-Castellanos, D., Larrasoaña, J.C., 2015. Quantifying the post-tectonic topographic evolution of closed basins: The Ebro basin (northeast Iberia). Geology 43, 663-666.

García-Castellanos, D., Vergés, J., Gaspar-Escribano, J., Cloetingh, S., 2003. Interplay between tectonics, climate, and fluvial transport during the Cenozoic evolution of the Ebro Basin (NE Iberia). Journal of Geophysical Research: Solid Earth 108, 2347.

Gómez-Ortiz, D., Tejero-Lopez, R., Babın-Vich, R., Rivas-Poncé, A., 2005. Crustal density structure in the Spanish Central System derived from gravity data analysis (central Spain). Tectonophysics 403, 131–149.

González de Vallejo, L.I., 2002. Ingeniería geológica. Pearson Prentice Hall, 744 pp.

Gosse, J.C., Phillips, F., 2001. Terrestrial in situ cosmogenic nuclides: theory and application. Quaternary Science Reviews, 20, 1475-1560.

Granger, D.E., Muzikar, P.F., 2001. Dating sediment burial with in situ-produced cosmogenic nuclides: theory, techniques, and limitations. Earth and Planetary Science Letters 188, 269-281.

He, P., Wang, X., Song, C., Wang, Q., Deng, L., Zhong, S., 2017. Cenozoic evolution of the Western Qinling Mt. Range based on thermochronologic and sedimentary records from the Wudu Basin, NE Tibetan Plateau. Journal of Asian Earth Sciences 138, 484-494.

Heidarzadeh, G., Ballato, P., Hassanzadeh, J., Ghassemi, M.R., Strecker, M.R., 2017. Lake overspill and onset of fluvial incision in the Iranian Plateau: Insights from the Mianeh Basin. Earth and Planetary Science Letters 469, 135-147.

Heisinger, B., Lal, D., Jull, A. J. T., Kubik, P., Ivy-Ochs, S., Knie, K. and Nolte, E., 2002a. Production of selected cosmogenic radionuclides by muons: 2. Capture of negative muons, Earth and Planetary Science Letters 200, 357–369.

Heisinger, B., Lal, D., Jull, A. J. T., Kubik, P., Ivy-Ochs, S., Neumaier, S., Knie, K., Lazarev, V. and Nolte, E., 2002b. Production of selected cosmogenic radionuclides by muons 1. Fast muons, Earth and Planetary Science Letters 200, 345-355.

Krijgsman, W., Garcés, M., Langereis, C.G., Daams, R., van Dam, J., van der Meulen, A.J., Agustí, J., Cabrera, L., 1996. A new chronology for the middle to late Miocene continental record in Spain. Earth and Planteray Science Letters 142, 367-380.

Lal, D., 1991. Cosmic ray labeling of erosion surfaces: in situ nuclide production rates and erosion models. Earth and Planetary Science Letters, 104, 424-439.

Lal, D., Arnold, J.R., 1985. Tracing quartz through the environment. Proceedings of the Indian Academy of Sciences-Earth and Planetary Sciences, 94, Issue 1, pp. 1-5.

Mather, A.E., 2000. Adjustment of a drainage network to capture induced base-level change: an example from the Sorbas Basin, SE Spain. Geomorphology 34, 271-289.

Mather, A.E., Stokes, M., Whitfield, E., 2017. River terraces and alluvial fans: The case for an integrated Quaternary fluvial archive. Quaternary Science Reviews 166, 74-90.

Mediavilla, R.U., Dabrio, C.J., 1989. Análisis sedimentológico de los conglomerados de Tariego (Unidad 4, Neógeno de la depresión del Duero). Studia Geologica Salmanticensia, Extraordinario No. 5, 293-310.

Mediavilla, R., Dabrio, C.J., Martín-Serrano, A., Santisteban, J.J., 1996. Lacustrine Neogene systems of the Duero Basin: evolution and controls. In: Friend, P.F., Dabrio, C.J. (Eds.), Tertiary Basins of Spain: the stratigraphic record of crustal kinematics. Cambridge University Press, Cambridge, pp. 228-236.

Moreno, D., Falguères, C., Pérez-González, A., Duval, M., Voinchet, P., Benito-Calvo, A., Ortega, A.I., Bahain, J.J., Sala, R., Carbonell, E., Bermúdez de Castro, J.M., Arsuaga, J.L., 2012. ESR chronology of alluvial deposits in the Arlanzón valley (Atapuerca, Spain): Contemporaneity with Atapuerca Gran Dolina site. Quaternary Geochronology 10, 418-423.

Moreno, D., Benito-Calvo, A., Falguères, C., Voinchet, P., Pérez-González, A., 2016. Preliminary Electron Spin Resonance (ESR) dating of Arlanza valley (NE Duero Basin, Burgos, Spain). XIV Reunión Nacional de Geomorfología, abstracts volume, Málaga, 391-398.

Nishiizumi, K., 2004. Preparation of ^{26}Al AMS standards. Nuclear Instruments and Methods in Physics Research Section B 223, 388-392.

Paola, C., Heller, P.L., Angevine, C.L. 1992. The large-scale dynamics of grain size variation in alluvial basins, 1: Theory. Basin Research 4, 73–90.

Pazzaglia, F.K. 2003. Landscape evolution models. Developments in Quaternary science 1, 247-274.

Pérez-González, A., 1982. El Cuaternario de la región central de la Cuenca del Duero y sus principales rasgos geomorfológicos, I Reunión sobre la Geología de la Cuenca del Duero. IGME, Salamanca, pp. 641-659.

Richardson, N.J., Densmore, A.L., Seward, D., Fowler, A., Wipf, M., Ellis, M.A., Yong, L., Zhang, Y., 2008. Extraordinary denudation in the Sichuan Basin: Insights from low-temperature thermochronology adjacent to the eastern margin of the Tibetan Plateau. Journal of Geophysical Research: Solid Earth, 113, B04409.

Rixhon, G., Braucher, R., Bourlès, D., Siame, L., Bovy, B., Demoulin, A., 2011. Quaternary river incision in NE Ardennes (Belgium)–Insights from 10Be/26Al dating of river terraces. Quaternary Geochronology, 6 (2), 273-284.

Rodés, Á., Pallàs, R., Ortuño, M., García-Melendez, E., Masana, E., 2014. Combining surface exposure dating and burial dating from paired cosmogenic depth profiles. Example of El Límite alluvial fan in Huércal-Overa basin (SE Iberia). Quaternary Geochronology, 19, 127-134.

Rodés, A., Pallàs, R., Braucher, R., Moreno, X., Masana, E., Bourlés, D.L., 2011. Effect of density uncertainties in cosmogenic ^{10}Be depth-profiles: Dating a cemented Pleistocene alluvial fan (Carboneras Fault, SE Iberia). Quaternary Geochronology 6, 186-194.

Rodríguez-Rodríguez, L., Antón, L., Pallàs, R., García-Castellanos, D., Jiménez-Munt, I., Pastor-Martín, C., 2020. A GIS method to identify flat surfaces and restore relict fluvial long-profiles from terrace remnants gives new clues on how large basins respond to endo-exorheic transitions (Duero Basin, Iberian Peninsula). Earth Surface Processes and Landforms 45 (4), 1013-1027.

Santisteban, J.I., Schulte, L., 2007. Fluvial networks of the Iberian Peninsula: a chronological framework. Quaternary Science Reviews 26, 2738-2757.

Santisteban, J.I., Alcalá, L., Mediavilla, R.M., Alberdi, M.T., Luque, L., Mazo, A., Miguel, I., Morales, J., Pérez, B., 1997. El Yacimiento de Tariego de Cerrato: El inicio de la red de drenaje actual en el sector central de la Cuenca del Duero. Cuadernos de Geología Ibérica 22, 431-446.

Schaller, M., Ehlers, T.A., Stor, T., Torrent, J., Lobato, L., Christl, M., Vockenhuber, C., 2016a. Spatial and temporal variations in denudation rates derived from cosmogenic nuclides in four European fluvial terrace sequences. Geomorphology 274, 180-192.

Schaller, M., Ehlers, T.A., Stor, T., Torrent, J., Lobato, L., Christl, M., Vockenhuber, C., 2016b. Timing of European fluvial terrace formation and incision rates constrained by cosmogenic nuclide dating. Earth and Planetary Science Letters 451, 221-231.

Silva, P.G., Roquero, E., López-Recio, M., Huerta, P., Martínez-Graña, A.M., 2017. Chronology of fluvial terrace sequences for large Atlantic rivers in the Iberian Peninsula (Upper Tagus and Duero drainage basins, Central Spain). Quaternary Science Reviews, 166, 188-203.

Soil Survey Staff, 2015. Illustrated guide to soil taxonomy, version 2. U.S. Department of Agriculture, Natural Resources Conservation Service, National Soil Survey Center, Lincoln, Nebraska. USDA, 2015. Illustrated guide to soil taxonomy

Spencer, J.E., Pearthree, P.A., 2001. Headward erosion versus closed-basin spillover as alternative causes of Neogene capture of the ancestral Colorado River by the Gulf of California. In Young, R.A., Spamer, E.E., (Eds.), The Colorado River: Origin and Evolution: Grand Canyon, Arizona, Grand Canyon Association Monograph 12, p. 215–222.

Soria-Jáuregui, Á, Jiménez-Cantizano, F., & Antón, L. (2019). Geomorphic and tectonic implications of the endorheic to exorheic transition of the Ebro River system in northeast Iberia. Quaternary Research, 91 (2), 472-492.

Stokes, M., Mather, A.E., Harvey, A.M., 2002. Quantification of river-capture-induced base-level changes and landscape development, Sorbas Basin, SE Spain. Geological Society, London, Special Publications 191, 23-35.

Stokes, M., Mather, A.E., Rodés, A., Kearsey, S., Lewin, S., 2018. Anatomy, age and origin of an intramontane top basin surface (Sorbas Basin, Betic Cordillera, SE Spain). Quaternary1 (2), 15.

Stone, J., 2000. Air pressure and cosmogenic isotope production. Journal of Geophysical Research, 105, 23753-23759.

Struth, L., Garcia-Castellanos, D., Viaplana-Muzas, M., Vergés, J., 2019. Drainage network dynamics and knickpoint evolution in the Ebro and Duero basins: From endorheism to exorheism. Geomorphology 327, 554-571.

Torrent, J., 1976. Soil development in a sequence of river terraces in northern Spain. CATENA, 3 (1), 137-151.

Whipple, K.X., 2001. Fluvial landscape response time: how plausible is steady-state denudation? American Journal of Science 301 (4–5), 313–325.

Whipple, K.X., Tucker, G.E., 1999. Dynamics of the stream power river incision model: implications for height limits of mountain ranges, landscape response time scales and research needs. Journal of Geophysical Research 104, 17661–17674.

Whittaker, A.C., Boulton, S.J. 2012. Tectonic and climatic controls on knickpoint retreat rates and landscape response times. Journal of Geophysical research 117, F02024.

Yu, X., Guo, Z., Fu, S., 2015. Endorheic or exorheic: differential isostatic effects of Cenozoic sediments on the elevations of the cratonic basins around the Tibetan Plateau. Terra Nova 27, 21-27.

Supplementary material: In situ density determination of fluvial terrace units

As density values assigned to fluvial sediments might have a strong impact in the final age model (Rodés et al., 2011), direct measurements were performed in the field for the various materials identified (Table I). Three types of density estimations were done (Figure 1): (i) the Archimedes' principle for bounded fluvial materials; (ii) driving a metal tube of known dimensions in unbound fluvial materials; and (iii) carving a rectangular or cylindrical prism. The first one was applied in the case of cohesive and/or heavily cemented (calcrete) gravel and sand materials: we inferred the sample volume by comparing the weight in air of a chunk of bounded sediments with the weight of the same sample (wrapped in plastic film) submerged in water, using a dynamometer (Figure 1A). In the case of unbound sandy materials, we drove a tube of known dimensions to obtain a density estimation from the ratio between the mass of material collected by the tube and the inner volume of the tube. Finally, the carving method was employed to measure the density of sand and gravel sediments displaying moderate cohesion. In this case, rectangular and cylindrical prisms were carved in order to obtain a density estimation from the ratio between the mass of material extracted and the volume of the shape carved. Volumes were determined either from the void dimensions in rectangular prisms or the volume of water needed to fulfill cylindrical prisms (a plastic bag was used to avoid water infiltration) (Figure 1B to 1E). Twenty-three density measurements were performed in the field obtaining values in the range 1.49–2.31 $g·cm^{-3}$ and providing an average density value of 1.72 ± 0.2 $g·cm^{-3}$. Based on these results, a range of density values of 1.52–1.92 $g·cm^{-3}$ has been used in the models, which is in good agreement with reference density values provided for dense coarse granular soils in some engineering manuals (e.g. González de Vallejo, 2002).

Table I.- Density estimations based on direct field measurements during the sampling campaign at the Duero fluvial terrace staircase, in June 2016 (C- pedogenic calcrete).

Terrace level	Sampling site	Method	Mass (g)	Volume (cm^3)	Type of material	Density ($g·cm^{-3}$)
T2	P88_ARE	Archimedes' principle	2125	1425	Cemented sand (C)	1.49
		Archimedes' principle	1650	900	Cemented fine gravel (C)	1.83
		Shape carving (rectangular)	1050	700	Gravel and sand	1.50
		Shape carving (rectangular)	750	455	Gravel and sand	1.65
		Shape carving (rectangular)	750	423	Gravel and sand	1.78
T3	P04_BAR	Archimedes' principle	4875	2925	Cemented gravel and sand (C)	1.67
		Archimedes' principle	4425	2750	Cemented sand (C)	1.61
		Archimedes' principle	4800	2850	Cemented coarse gravel (C)	1.68
		Shape carving (rectangular)	3475	2160	Dry sand	1.61

		Shape carving (rectangular)	8000	5720	Dry sand	1.40
		Shape carving (rectangular)	5100	2720	Dry sand	1.88
T10	P14_FON	Archimedes' principle	3000	1875	Cemented gravel (C)	1.60
		Archimedes' principle	1625	1050	Cemented gravel	1.55
T11	P84_SOL	Tube driving (by hand)	250	147.5	Cross-bedded sand	1.69
		Tube driving (by hammer)	375	173.42	Wet medium sand with granules	2.16
		Tube driving (by hammer)	450	238.76	Wet medium sand with granules	1.88
		Archimedes' principle	2950	1825	Cemented gravel and sand	1.62
		Tube driving (by hammer)	450	261.38	Wet sand	1.72
T12	P38_ISI	Shape carving (rectangular)	3600	1560	Wet sand and gravel with clay matrix	2.31
		Archimedes' principle	2925	1750	Cemented sand, sparse gravels (C)	1.67
		Tube driving (by hammer)	350	213.6	Wet cohesion less sand	1.64
		Tube driving (by hammer)	375	238.7	Wet cohesion less sand	1.57
		Shape carving (cylindrical)	1450	600	Wet sand and gravel	2.42

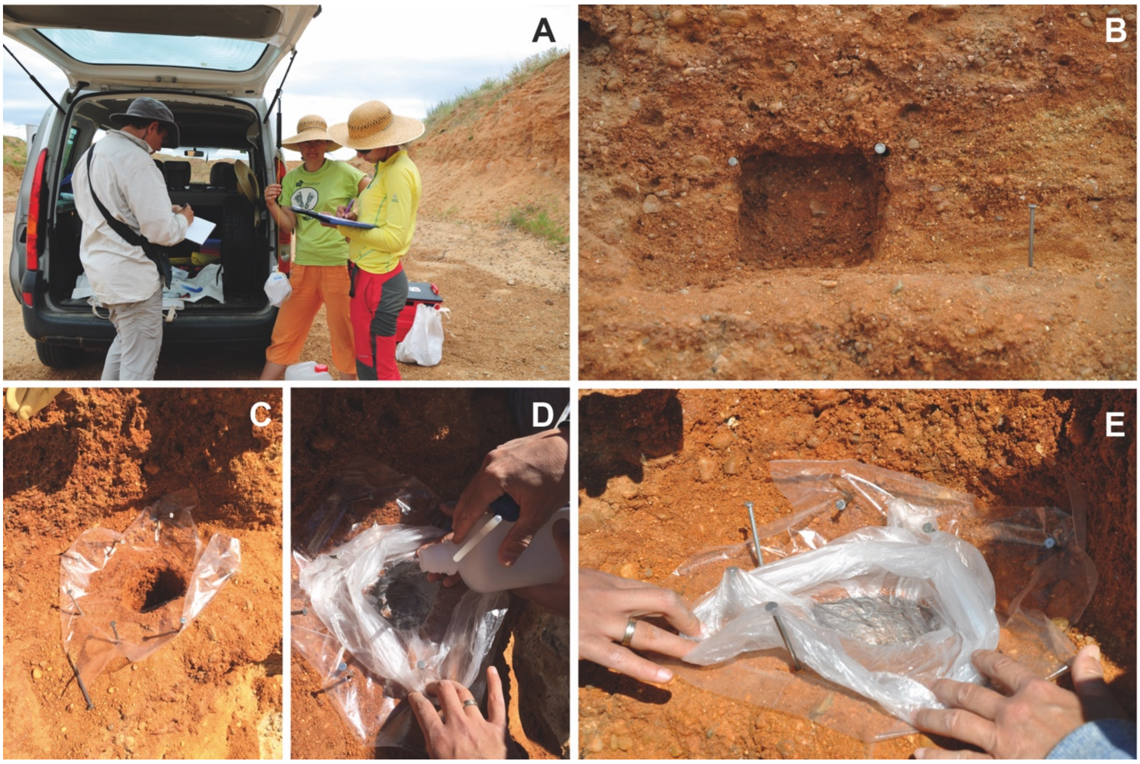

Figure 1.- Examples of density estimations of fluvial sediment materials done in the field. (A) Volume determinations in cemented sediments were done using a dynamometer to compare sample's weight in air and submerged in water. (B) Volume of poorly cemented sediments showing enough cohesion as to allow carving a polyhedral shape of measurable dimensions. (C-E) Example of volume determination carving a cylindrical shape. In this case, we used a thin plastic bag to avoid infiltration and recover the volume of water needed to fulfill the cylindrical shape (the water volume was measured with a graduated column not visible in the pictures).